Early post-rift depositional systems of the Central Atlantic
Lower and Middle Jurassic of the Essaouira-Agadir Basin, Morocco

Duval-Arnould, Aude; Schröder, Stefan; Charton, Rémi ; Joussiaume, Rémi ; Razin, Philippe ; Redfern, Jonathan

DOI
10.1016/j.jafrearsci.2021.104164

Publication date
2021

Document Version
Accepted author manuscript

Published in
Journal of African Earth Sciences

Early post-rift depositional systems of the Central Atlantic: Lower and Middle Jurassic of the Essaouira-Agadir Basin, Morocco.

Aude Duval-Arnould[a]; Stefan Schröder[a]; Rémi Charton[a,b], Rémi Joussiaume[c], Philippe Razin[c], Jonathan Redfern[a]

[a] University of Manchester, Department of Earth and Environmental Sciences, North Africa Research Group, M13 9PL, Manchester, UK. aude.duval-arnould@manchester.ac.uk; stefan.schroeder@manchester.ac.uk; jonathan.redfern@manchester.ac.uk

[b] Department of Geoscience and Engineering, Delft University of Technology, P.O. Box 5048, 2600 GA, Delft, The Netherlands. r.j.g.charton@tudelft.nl

[c] ENSEGID Bordeaux INP, Pessac, France. remi.joussiaume@gmail.com; Razin@ensegid.fr

Abstract

Passive margins are traditionally regarded as tectonically quiescent, however the increasing recognition of significant post-rift tectonic uplift along their flanks offers an important control on sediment delivery. The most extensive record of the early post-rift succession of the Central Atlantic Margin (CAM) is found in the Lower and Middle Jurassic outcrops of the Essaouira-Agadir Basin (EAB). This important succession is characterised by alternating deposition of marine carbonates and paralic siliciclastics that correlate with periods of tectonic activity along the margin, rejuvenating sediment input to the basin. Field observations, well data and petrographic analysis are integrated into a coherent sedimentological model, correlated across the basin within a sequence stratigraphic framework. Comparison is drawn with equivalent dated units in the Central High Atlas, which allows a constraint on the regional versus local tectonostratigraphic evolution.

In the EAB, Upper Sinemurian to Lower Pliensbachian open marine ramp carbonates record an initial transgression. They are only preserved locally in the north of the basin, below a

major fluvial erosion surface that is regionally traceable across the basin and incisive into the Pliensbachian CAMP basalts or Triassic sediments. In the Central High Atlas (CHA), the correlative fluvial erosive event has been dated as Toarcian in age. This influx of siliciclastic sediments is interpreted to have been sourced from the Meseta and/or the Anti-Atlas, supporting recent apatite-fission track thermochronology that indicates erosional exhumation at this time.

During the Upper Toarcian, a regional carbonate platform, dominated by peritidal deposits, developed across the EAB in response to renewed marine transgression. Facies include oolitic and bioclastic grainstones, crystalline dolomite, stromatolites and dissolution breccias or evaporites. Overlying Middle Jurassic shallow-marine and fluvial siliciclastics encroached from south of the basin (possibly related to a potential source area in the Anti-Atlas), while to the north shallow marine carbonates dominated. These observations evidence the role of tectonic movements of the hinterland during a passive margin phase as a mechanism to trigger forced regressions, compensating the effect of eustasy.

Key words: Carbonate sedimentology, Post-rift, Mixed system, Jurassic, Atlantic Margin, Western High Atlas, Sequence Stratigraphy, Passive Margins

1 Introduction

Although passive margins are generally regarded as tectonically quiescent, there is increasing realization of significant post-rift tectonic uplift along several rifted margins (e.g. Ghorbal et al., 2008; Wildman et al., 2015; Japsen et al., 2016). Such uplift movements not only modify the topography along the margin, but lead to punctuated increase in erosion and sediment delivery to the surrounding basins. The passive margin sedimentary succession therefore offers a potential record of margin exhumation and landscape evolution (Burke and Gunnell, 2008). Quantifying uplift-related sediment input is important to predict the location and nature of potential reservoirs for economic resources such as hydrocarbons.

The Essaouira-Agadir Basin (EAB) offers a rare outcrop window to constrain the links between post-rift tectonic uplift and mixed carbonate-silicicastic sedimentation. The basin is located on the eastern flank of the Central Atlantic Margin (CAM) of Morocco and records its syn- and post-rift evolution. Alpine uplift now exposes the most complete Mesozoic succession along the entire CAM. It comprises interbedded carbonates and siliciclastics (Ambroggi, 1963; Bouaouda, 1987; Peybernès et al., 1987), and variations in the sedimentation and the periodic siliciclastic influx in the basin result from increased denudation in the hinterland of the EAB.

The early post-rift stage of the eastern CAM was previously interpreted to record fairly monotonous thermal subsidence, with extensive carbonate platforms deposited over rifted basement (Lehner and De Ruiter, 1977; Le Roy, 1997; Frizon de Lamotte, 2000; Le Roy and Piqué, 2001 and Guiraud et al. 2005). More recent studies suggest that the adjacent non-rifted continental crust was more tectonically active, with high rates of exhumation in the Western Messeta (e.g Ghorbal et al., 2008) and the Anti-Atlas during the Jurassic (Fig. 1), which influenced sedimentation (Sehrt, 2014; Gouiza et al., 2017; Charton et al., 2018).

This paper (1) refines the sedimentological understanding and establishes the local and regional trends in carbonate deposition in the EAB, recognizing the scales of transgressive-regressive cycles affecting the sedimentation and identifying the lateral distribution, (2) integrates the sections logged at basin scale within a sequence stratigraphic framework to identify key surfaces and determine the sedimentological controls on the facies variations, (3) places the results into a regional context and assesses the controls of siliciclastic versus carbonate sedimentation along the western Moroccan margin. Finally, the EAB is compared with the Central High Atlas (CHA) basin to (4) assess evidence for erosional exhumation and tectonic uplift during the Lower and Middle Jurassic across both basins.

2 Geological setting

2.1 Structural evolution and syn-rift sedimentary architecture

The Western High Atlas (WHA) comprises the EAB and the Massif Ancien de Marrakech (MAM). It inherited its geometry following the Variscan Orogeny (Piqué et al., 1998; Hafid et al., 2006; Lanari et al., 2020) and subsequent Triassic rifting, the latter associated with opening of the Central Atlantic (Favre and Stampfli, 1992, Hafid, 2000; Hafid et al., 2000; Domènech et al., 2015). The rift zone faulted older Precambrian-Palaeozoic basement and reactivated structures inherited from the Variscan orogeny and potentially older lineaments. During the Variscan, the CHA experienced deformation along shear zones showing two main orientations, N20–45°E and N70–90°E, which later acted as zones of weakness during Triassic rifting (Pique et al., 1998; Le Roy and Piqué, 2001; Laville et al., 2004). N-S to NNE-SSW westward-dipping half-grabens have been interpreted (Medina, 1988; Bouatmani et al., 2003) linked by E-W transfer faults, which are believed to be reactivated Variscan thrust faults (Laville and Piqué, 1992).

Rifting of the CAM began in the Ladinian (Middle Triassic) (Schettino and Turco, 2009, 2011), and terminated with the formation of the first oceanic crust in the proto-Atlantic, during the Sinemurian (Pique et al., 1998; Hafid, 2000). In the Argana Valley (Fig. 2), the basin has over 2000 m of continental, dominantly red-coloured, siliclastic deposits, lacustrine shale, evaporite and basalt fill. (Olsen et al., 2003; Mader et al., 2011). Although the structural style during Triassic deposition is debated (Hofmann et al., 2000; Baudon et al., 2012), the previous studies all agree on minimal tectonic influence on Lower Jurassic sedimentation.

The basin suffered gradual sag subsidence until the Alpine/Atlas Inversion, that lasted from the Upper Cretaceous to the Neogene (Hafid, 2000; Hafid et al., 2006). This reactivated faults, uplifting and folding the exposed Mesozoic sections.

2.2 CAMP Basalts

In the western part of the EAB, (e.g. Jebel Amsittène and in offshore wells) the Central Atlantic Magmatic Province (CAMP) basaltic event is regionally used as the stratigraphic marker for the base of the Jurassic. The basalt flows were emplaced during the final phase of rifting that initiated the break-up of the Atlantic. The CAMP magmatism spans about 10 Ma, with a 600 000 years to 1 Ma peak of activity dated by radiometric methods to around

199 Ma (Fiechtner et al., 1992; Marzoli et al., 1999; Palfy et al., 2000; Knight at al., 2004; Nomade et al., 2007; Verati et al., 2007; Davies et al., 2017). The link between the Triassic-Jurassic mass extinction and the CAMP basalts has been extensively studied and refined (Whiteside et al., 2007; Blackburn et al., 2013; Davies et al., 2017), although there is an ongoing debate as to whether the CAMP volcanism predates (Marzoli et al., 2004, Nomade et al., 2007; Whiteside et al., 2007) or postdates (Olsen et al., 2003; Whiteside et al., 2007) the Triassic-Jurassic boundary. For the purpose of this paper, the CAMP magmatism is considered synchronous with the Triassic-Jurassic boundary, and in the absence of direct age constraints on the overlying deposits, these are regarded as lowermost Jurassic.

2.3 Lithostratigraphy

The Lower Jurassic stratigraphy of the EAB has historically been described based on lithostratigraphy (Fig.3) (e.g. Roch, 1930; Ambroggi, 1963; Duffaud, 1960; Adams, 1979; Adams et al., 1980; Peybernes et al., 1987; Du Dresnay, 1988; Bouaouda, 2007). This approach has been retained in this paper due to a lack of precise dating for most of the syn-rift and early post-rift formations. Adams and co-authors (1980) defined three main lithostratigraphic units and distinguished them into the Amsittène and Tamarout and Ameskhoud formations. The older Arich Ouzla Formation was subsequently separated from the Amsittene Formation and named by Peybernes et al. (1987). The formations rest upon the CAMP Basalts that mark the Triassic/ Jurassic boundary.

Arich Ouzla Formation

Lowermost Jurassic carbonates have been ascribed to the Arich Ouzla Formation (Fm) (Fig.3). Onshore, this unit is only locally preserved in the core of the Amsittène Anticline (Fig. 2), and consist of dolomitic carbonates. This succession rests on Triassic red mudstones and evaporites (Du Dresnay; 1988). The Arich Ouzla Fm has been dated as Sinemurian to Lower Pliensbachian on the basis of brachiopod fauna (Duffaud, 1960; Peybernes et al., 1987).

Amsittene Formation

Red to purple coloured siliciclastic deposits of the Amsittène Formation thicken to the NE and have a generally erosive base, resting upon basalts or Triassic continental deposits

(Tixeront, 1974). A Toarcian age was determined by superposition, between the underlying Arich Ouzla Fm (Upper Sinnemurian - Lower Pliensbachian) and the overlying Tamarout Farmation (Toarcian; Peybernes et al., 1987; Du Dresnay; 1988). The Amsittène Fm passes gradationally upwards into the Tamarout Fm, through two transitional environments, a coastal plain or a sabkha.

Tamarout Formation

The Tamarout Formation contains up to 400 m of dolomites and dolomitic limestones, with associated breccia horizons or evaporites (Ambroggi, 1963; Bouaouda, 1987, 2007). This unit is laterally heterogeneous and the proportion of evaporites, stromatolites or siliciclastic material varies around the basin. Brachiopods (*Zeilleria lycetti;* Adams et al., 1980*,* and *Terebretula withakeri?;* Determination G. Dubar in Ambroggi, 1963) place the upper part of this formation into the Toarcian (Ambroggi, 1963).

Ameskhoud Formation

The Ameskhoud Fm follows the Tamarout Fm in the south and west of the EAB (Agadir Basin). It is composed of red mudstones and siltstones alternating with sandstones and conglomerates (Ambroggi, 1963). In the Essaouira Basin and offshore EAB, this formation is laterally equivalent to a thick dolomitic interval (Fig. 4) initially ascribed to the Tamarout Fm, later renamed the Id Ou Moulid Fm (Peybernes et al. 1987). The Ameskhoud Fm is dated as Aalenian to Bathonian/Callovian in age (Adams et al., 1980; Du Dresnay, 1988; Bouaouda et al., 2007), based on its relative position, bracketed between the Toarcian Tamarout Fm and the overlying Ouanamane Fm, the basal age of which has been interpreted as Bathonian based on foraminifera (Bouaouda et al., 2007 and references therein). New biostratigraphic evidence indicates that a lower Callovian age cannot be excluded for the Ouanamane Fm (Duval-Arnould, 2019).

3 Depositional systems

Stratigraphic units are described and interpreted successively from bottom to top. Above the basal, carbonate-dominated Arich Ouzla Fm, the succession displays two main lithological cycles from coarse siliciclastics (Amsittene Fm) to carbonates (Tamarout Fm), followed by a return to fine-grained siliciclastics (Ameskhoud Fm). The study of the facies associations (FA) was conducted to identify the elements and processes involved, and to identify the different depositional environments and their evolution. Individual lithofacies and their facies associations (FAs) are outlined in the figures 5, 7, 10, 12 and 15. Nomenclature is as follows: LF[X][n_a] are lithofacies (LF) grouped into FA[n_b] facies associations (FA), with X an abbreviation of the associated formation name and n_a and n_b independant increasing numbers.

3.1 Methodology

The data presented in this study derive from 7 georeferenced (GPS locations given in Annex) sections that have been logged at high resolution across the EAB (Fig. 2). Samples were collected every 2 m on average for the Lower Jurassic and fewer samples collected for the Middle Jurassic. Petrographic analyses were conducted on the two carbonate formations: 18 thin sections for the Arich Ouzla Fm and 22 thin sections of the Tamarout Fm. Microfacies analyses were based on texture, diagnostic grains, grain type quantification, sedimentary structures and bioturbation. The carbonate facies and microfacies descriptions were based on the Embry and Klovan (1971) extension to the Dunham (1962) classification, with the introduction of the terms floatstones and rudstones for facies with elements larger than 2mm. The siliciclastic lithofacies descriptions were based on textural classification and sedimentary structure observations. The grain size grades follow the scale defined by Wentworth (1920) and the textural classes from Folk (1980). The fabric was also taken into consideration where necessary and distinguished following the nomenclature from Farrell et al. (2012). For mixed facies, the lithofacies name follows the classification of the dominant rock-type with a prefix indicating the grain size of the subordinate siliciclastic component in the case of carbonate-dominated facies; or for siliciclastic-dominated facies, the prefix dolomitic or calcareous is applied where a noticeable amount (above 5%) of calcium carbonate is present. Both carbonate and siliciclastic facies were analyzed at macro scale, and the bed geometries, lithologies, sedimentary structures, fossil content and bioturbation features have been described and interpreted.

At outcrop scale, the thicknesses, lateral extent and cyclicity of the different beds were recorded to get a better understanding of the depositional environment. The onshore wells

Timsilline-1 (TMS-1) and Essaouira-1 (ESS-1); and the offshore wells Essaouira-1X (ESR-1X), Essaouira West-1bis (ESW-1bis) and DSDP site 547 (Fig. 2) reached the base of the Lias and show stratigraphy equivalent to the Arich Ouzla Fm. Well data provided further biostratigraphic constraints and constrained the offshore variations of the formations studied.

3.2 Facies analysis

3.2.1 Arich Ouzla Formation

The Arich Ouzla Fm is the oldest Mesozoic carbonate unit identified in the basin. This formation is observed onshore in the core of the Jbel Amsittène (Arich Ouzla and Ida Ou Azza salt mines) in the North of the EAB; a similar unit occurs in the Tidzi diapir and in well Essaouira-1 (ESS-1). This formation thickens towards the North (well ESS-1), which may be an indication of the South-North basin orientation (Dresnay, 1988).

3.2.1.1 Depositional architecture

In total, 84 m of the Arich Ouzla Fm was logged in the NE part of the outcrops surrounding the Arich Ouzla salt mine. The lower boundary of the formation is not visible, but the location of the salt mine suggests only 1 to 6 m of cover between the carbonates and underlying Triassic red mudstones and evaporites. The formation is composed of three lithologic units in this locality.

Unit I: Fine-grained carbonates

Unit I represents the basal part of the formation, which rest on top of Triassic red mudstones. It is highly dolomitic and present a very vuggy aspect on the outcrop. It is principally composed of oolitic and peloidal sediments (LFAO1 and LFAO2) (Fig. 5). The top 7 m of this unit records horizontal laminations and horizontal stylolites and is characterised by a darker colour and an associated strong kerogenic smell.

Unit II: Oncoidal sequence

The base of this unit is very dolomitic and made of oncoidal FST and RST with abundant shell fragments (LFAO2) (Fig. 5 and 6). The middle part consists of oncoidal and peloidal FST (Fig. 6, b) and PST with very abundant crinoids (Fig. 6, c), shell fragments (Fig. 6, d) and some belemnites, *Trichites* bivalve shells, and gastropods (LFAO3, LFAO4 and LFAO5). Ammonites have been observed, but their poor preservation prevented further identification. The upper part of this unit displays some solitary corals and coral fragments in smaller (up to 1cm) oncoid-dominated facies.

Unit III: Crystalline dolomite

Unit III is composed of 22 m of crystalline dolomite (LFAO6). The lower part of the unit is thinly bedded and contains abundant horizontal stylolites. The bulk of the unit is made of patches of yellow, pink, purple and white dolomite. The upper part of this unit is strongly bioturbated, and intensly weathered. Abundant small fractures and vugs are present.

3.2.1.2 Lithofacies description

3.2.1.2.1 Lithofacies LFAO1

Description - Lithofacies LFAO1 is essentially composed of strongly recrystallized oolitic and peloidal packstones and grainstones (Fig. 5). Locally, less recrystallized beds still present micritic ooids and peloids with a matrix of euhedral and subhedral dolomite crystals. Oncoids, crinoids, and coral fragments are rare.

Interpretation - The lithofacies is dominated by ooids and peloids. The apparent homogeneous grain size, allochem roundness and the grain-supported texture indicate continuous reworking by high energy currents which sorted the grains and prevented accumulation of mud. Peloidal and oolitic grainstone facies are both diagnostic of shallow platform interiors, in inner and mid-ramps (Halley et al. 1983; Flügel, 2010) .

3.2.1.2.2 Lithofacies LFAO2

Description - Lithofacies LFAO2 is partially to fully dolomitized and made of oncoidal PST, FST and RST (Fig. 5). Where dolomitization is only partial, the main elements consist of coated grains, oncoids, peloids and thin shell fragments with a micrite matrix (Fig. 6, a). Ellipsoidal non-laminated oncoids and coated grains are associated with thin shell fragments, whereas more massive oncoids formed without distinguishable nuclei, or around more rounded bioclasts or even some foraminifera. Very small gastropods and <10% very fine quartz are associated.

Interpretation - The presence of shallow and larger oncoids indicates a relatively low energy environment. Very thin shell fragments suggest some currents, but the energy level of the system was limited. The co-existence in the same facies of mature oncoids and non-coated shell fragments indicates some limited transport of allochems.

3.2.1.2.3 Lithofacies LFAO3

Description - Lithofacies LFAO3 is composed of oncoidal rudstones with large elliptical and concentric spongiostromate oncoids, small peloids, and shell fragments (Fig. 5). Long crinoid stems and crinoid ossicles are abundant. The matrix is composed of micrite and microspar with up to 10% very fine quartz grains.

Interpretation - The very abundant large spongiostromate oncoids indicate a low-energy environment, which must have been relatively open marine due to the relative abundance of crinoids. Low energy allowed significant micrite accumulation, but the presence of bioclasts indicates limited or intermittent reworking.

3.2.1.2.4 Lithofacies LFAO4

Description - Lithofacies LFAO4 is defined by crinoid floatstones (Fig. 5), dominated by crinoids, coated grains, and associated shell fragments and very fine quartz grains. The matrix is composed of micrite and microspar. Belemnites and ammonites are present, but their poor preservation impeded determination.

Interpretation - The abundant coated grains and more limited oncoids of the lithofacies LFAO4 indicate either higher sedimentation rate or a higher energy environment compared to LFAO3. The high amount of crinoids stems and ossicles, as well as the presence of belemnites and ammonites, are characteristic of open marine environments and indicate some pelagic influence. The amount of peloids and micrite in this lithofacies also tends to indicate little reworking and low energy.

3.2.1.2.5 Lithofacies LFAO5

Description - Lithofacies LFAO5 is composed of bioclastic wackestones to floatstones (Fig. 5). It is dominated by shell fragments representing a diverse fauna, including occasional coral fragments, and coated grains (Fig. 5). Quartz content (<5%) is reduced relative to LFAO3 and LFAO4. Indeterminate belemnite fragments and ammonites are present. This facies is partially dolomitized.

Interpretation - The abundant shell fragments and coated grains in LFAO5 indicate constant water agitation (Flügel, 2010), at or above fair weather wave base. The micrite envelope around some of the grains is destructive, due to the action of microborers, most likely in a photic environment. The coral fragments indicate the proximity of either a lagoonal or a reefal environment, while ammonite and belemnite fragments reflect more open environmental conditions.

3.2.1.2.6 Lithofacies LFAO6

Description - Lithofacies LFAO6 is highly dolomitized (Fig. 5) and heavily fractured in outcrop. Locally the top of beds are highly bioturbated by *Thalassinoides*. The thin sections show some recrystallized shell fragments phantoms and euhedral and anhedral dolomite crystals.

Interpretation - Most of the sedimentary features and elements are indistinguishable due to the dolomitization. However, the presence of *Thalassinoides* indicates a marine origin (Gerard and Bromley, 2008), and the presence of shell fragment phantoms indicates that this lithofacies can be derived from LFAO5, where shell fragments were the main elements.

3.2.1.3 Facies association interpretation

3.2.1.3.1 FA1: Lagoonal carbonates (LFAO 1 and 2)

During the Jurassic, oncoids were frequently deposited across most carbonate shelf environments down to the basin (Flügel, 2010). However, the shallow oncoidal coated-grains, associated to peloidal grainstones with thin shell fragments (Fig.5) indicate a low energy environment, while the oolitic packstones indicate the proximity of a higher energy environment. The position of the Unit I in a transgressive sequence, between continental Triassic deposits and mid-ramp deposits of Unit II rather indicates a shallow lagoon environment of deposition. Oolitic and peloidal PST and GST also require a moderate to high energy environment. Unit I can be interpreted as lagoonal to upper-midramp deposits.

3.2.1.3.2 FA2: Midramp carbonates (LFAO 2 to 6)

In Unit II, the large size of the oncoids is due to lower water energy level. The presence of organisms related to a deeper environment (ammonites, belemnites, crinoids) (Fig.5) suggests that this unit was deposited further down-ramp. In the upper part of the unit, the association of corals to crinoids and smaller oncoids indicates an environment with higher energy, probably a midramp in the vicinity of a potential organic buildup.

In Unit III, the depositional features have been erased by dolomitization and the environment identification is impossible.

3.2.1.4 Regional variations

The offshore well drilled on site 547 by DSDP leg 79 reached the lower part of the Lower Jurassic, and found deeper-water facies further north of Essaouira. The occurrence of nanofossils *Involutina ticinensis* (Schweighauser) together with *Schizosphaerella punctulata* and *Schizosphaerella astrea* and the well-preserved foraminifera assemblages dominated by Nodosariids date cores 24 to 14 from the Well 547B as Late Sinemurian to Early Pliensbachian (Bernoulli and Kälin, 1984; Riegraf et al., 1984). These deposits are made of 77m black shales and pelagic limestones, directly overlying poorly dated stromatolitic boundstones (Steiger and Jansa, 1984). This interval was interpreted as a deeper pelagic environment. Associated limestone breccias and redeposited nodular limestones could derive from a shallower carbonate ramp equivalent to the Arich Ouzla Fm described in outcrop.

3.2.1.5 Transition to continental deposits

At the contact between the Arich Ouzla and Amsittene formations in the northern part of the Arich Ouzla salt mine, breccias are present at the top of the Arich Ouzla Fm. The breccias can be mapped locally and form a clear linear surface that separates the Arich Ouzla and Amsittène formations. It only extends laterally for a few metres. These breccias are made of very angular autochthonous limestones boulders and pebbles. The limestone elements show very little transport and are grain-supported, or floating in a fine to medium red sandstones matrix with occasional quartz granules and pebbles. These breccias are not associated to any faulting, but rather related to the erosion of the limestones before the time of deposition of the continental sediments.

3.2.2 Amsittène Formation

The Amsittène Fm outcrops in several localities around the EAB. The thickness of this formation across the basin varies between 80 and 140 m, pinching out to the NE along the Argana Valley close to Zaouiat Ouidmane (Tixeront, 1974). The channelized base is erosive, cutting into Paleozoic, Triassic, and older Jurassic deposits.

3.2.2.1 Depositional architecture

3.2.2.1.1 Tikki

In the outcrops of Tikki, located along the northern branch of the Tizi N'Test Fault (Fig. 2), part of the Amsittène Fm is composed of massive quartzite conglomerates (LFAT1) and interbedded sandstones (Fig. 7). Three conglomerate units can be distinguished (Fig. 9), separated by sandstone units (LFAT2 and LFAT3). The thickness of the conglomerate units may vary slightly laterally but the general organisation remains consistent along the outcrop. Horizons of pebbly sandstones (LFAT2) are present at the base and at the top of the two first conglomerates (LFAT1). The first conglomerate unit is 6 m thick and is separated from the second conglomerate unit by 10 m of fine to medium grained sandstones (LFAT2). The second conglomerates unit is 5 m thick and displays fining upward. It is separated from the third by 5 m of fine grained sandstones and mudstones. The third conglomerate is coarse-grained, poorly-sorted, and has a non-erosive base. This unit fines upward, from massive conglomerates at the base to horizontally stacked conglomerate sets with apparent cross-bedding and to cross-bedded conglomerate with sandstones lenses (LFAT2) towards the top. It is directly followed by medium and fine sandstones (LFAT3), rapidly grading into mudstones. Palaeocurrents mesurements are variable, pointing dominantly westward, with subordinate palaeocurrents to the east and south.

3.2.2.1.2 Askouti and Tizgui

In Askouti and Tizgui, the base of the Amsittène Fm is composed of channelized conglomerates (LFAT4) with sandstones. In Tizgui, this formation lies uncomformably on top of the CAMP basalts. The width of the riverbed is difficult to constrain due to the narrow exposition of the outcrops. In both locations, the conglomerate unit is composed of multiple conglomerate beds with a lenticular shape. The conglomerate unit is fining upward to coarse sandstones (LFAT5) then fine sandstones (LFAT6). It is followed by a mudstone and siltstone unit interbedded with thin very fine sandstones layers.

3.2.2.2 Lithofacies descriptions

3.2.2.2.1 LFAT1

Description - Lithofacies LFAT1 is a quartzite conglomerate composed of well rounded pebbles and cobbles up to 15 cm in diameter (Fig. 8, a, b). The conglomerates are polymodal, poorly sorted, mainly clast-supported, with dominantly quartzite pebbles and cobbles and rare basalts and metabasalts (Fig. 7). The pebbles are often pitted, the result of modern pebble impacts, that gives them a characteristic off-white colour. These conglomerates display erosive or non-erosive base, cross bedding and parallel laminations. Some sandstones lenses made of sub-angular finer material separate the conglomerates foresets and pick out the local cross-bedding (Fig.8, c).

Interpretation. - The lenticular cross stratified pebbly sandstones in the clast-supported conglomerate units suggest deposition in high-energy environments and can be interpreted as streamflow deposits (Nilsen, 1982). The cross-bedded sand lenses were deposited from waning traction currents (Miall, 1977, 1996; Blair, 1999). The massive conglomerates with good lateral continuity indicate unconfined aggradation (Nilsen, 1982). The non-erosive base of the third conglomerate, followed by an unstratified conglomerate unit is characteristic of non-cohesive debris flow deposits. Its large extent is indicative of a lobe deposit (Harvey et al., 2005).

3.2.2.2.2 LFAT2

Description - LFAT2 consists of medium to coarse-grained, poorly-sorted sandstones with pebbly horizons. This facies shows common planar cross-beds and small-scale (15-25 cm) trough cross-beddings with pebbles and cobbles concentrated at the base of some sets. Thin, cross-bedded, sandy horizons with granules are particularly common on top of the main conglomerate units.

Interpretation - Alternating couplets of cobble–pebble gravel and coarse or pebbly sand organised in cross-beds are characteristic features of sheetfloods deposits in waterlaid alluvial fans (Blair and McPherson, 2009). The cross-bedded sandstones are interpreted to be deposited by sheetflood from braided streams (Miall, 1977; Heward, 1978).

3.2.2.2.3 LFAT3

Description - Lithofacies LFAT3 is composed of poorly-sorted, fine-grained sandstones.This lithofacies consists in interbedded, horizontally stratified, fine-grained material, with no visible current features. These sheet-like sandstones are formed by a succession of thin individual beds (10-30 cm) with rare roots traces and occasional nodular beds and rootlets traces(Fig. 8, d).

Interpretation - These fine sandstone horizons incate less catastrophic discharge, carrying limited sediments. They can be interpreted as overland flow deposits, winnowed from adjacent lobes deposits (Blair and McPhesron, 2009). The nodules and rootlets are interpreted as paleosoils and indicate the presence of stabilizing vegetation.

3.2.2.2.4 LFAT4

Description - The red conglomerates in Askouti and Tizgui have an erosive base and are composed of quartzite and basaltic pebbles and cobbles. The conglomerates are up to 2m thick and present horizontal bedding and low-angle cross-beds (Fig. 7). The conglomerates are lenticular shaped and repeat through the stratigraphy. They present a pebble-supported base, with sub-rounded to sub-angular pebbles and cobbles. Their sorting is poor, but they locally contain matrix-supported lenses with aligned pebbles.

Interpretation - The erosive base and lenticular shape of the conglomerates indicate deposition by a confined flow. The presence of cross-bedding and low angle cross-bedding associated to the clean coarse sandstone matrix indicate deposition by a high energy streamflow.

3.2.2.2.5 LFAT5

Description - Lithofacies LFAT5 is composed of poorly-sorted, coarse-grained sandstones with granules (Fig. 7). The coarse sandstones are trough cross-bedded or have tabular and plannar cross-bedding. Subhorizontal beds of gravel-rich sediments are commonly intercalated in these deposits.

Intirpretation - The alternation of clean coarse sandstones and gravels horizons may indicate two different flow regime. This feature can happen in ephemeral streams or at the surface of longitudinal barforms as the result of a secondary transverse flow (Rust, 1972). The coarse sandstones at the top of fining-upward conglomerates which mainly exhibiting tabular cross-bed sets with planar cross-bedding can be interpreted as bed-load sheets deposited on bar crests. The coarse sand-wedges and lenses with planar cross-bedding and trough cross-bedding could also be interpreted as transverse bars or isolated active channel in sheltered part of the stream (Rust, 1972; 1977; Miall, 1977; Lunt and Bridge, 2004).

3.2.2.2.6 LFAT6

Description - Lithofacies LFAT6 are composed of medium and fine grained sandstones. The medium-grained sandstones present well-developed current ripples and horizontal bedding. The fine- to medium-grained sandstones exhibit migrating ripples with an average height of 2 cm. The migrating ripples in the sandstones are organised as sets, where the stoss side are not preserved for most of the sets.

Interpretation - The finer sediments and the formation and preservation of the ripples indicate a variation of the current strength. This facies is associated to a more protected environment within the river or due to waning of the flow and deposition on bar tops (Miall, 1996; Best et al, 2003).

3.2.2.2.7 LFAT7

Description - Lithofacies LFAT7 is composed of finely laminated red mudstones and siltstones alternating with more massive mudstones beds, up to 50 cm thick (Fig. 7). The mudstones and siltstones units alternate with thin beds or lenses of siltstones presenting occasional current ripples (Fig. 7, LFAT7).

Interpretation - The grain size of this lithofacies indicates a low-energy environment. The presence of occasional small current ripples and dominant horizontal laminations reflect suspension processes, with minor reworking (Lowe, 1988).

3.2.2.2.8 LFAT8

Description - Lithofacies LFAT 8 is composed of cm-thick beds of very fine-grained sandstones (Fig. 7, LFAT8). The very fine-grained sandstones grade upward to siltstone and display locally current ripples and flaser bedding.

Interpretation - The fining upward to siltstones and the presence of current ripples and flaser bedding indicate episodic flooding or intermittent flow (Martin, 2000).

3.2.2.2.9 LFAT9

Description - Lithofacies LFAT 9, composed of fine-grained sandstones sheets with sharp bases, low-angle tabular cross-bedding and climbing current ripples (LFAT9) is common. The fine sandstones beds are usually 30 to 40 cm thick and alternate with siltstones beds.

Interpretation - The sharp base and relatively coarser sediments of this lithofacies indicate deposition in higher energy settings compared to LFAT7 and LFAT8. The sedimentary features indicate a downstream ripple migration, and the climbing ripples suggest deposition by decelerating flow or fallout of sediments from suspension (Ashley et al., 1982), which is characteristic of flows associated with river floods.

3.2.2.2.10 LFAT10

Description - Lithofacies LFAT10 is composed of matrix supported conglomerates (Fig. 7, LFAT10) that form 40 cm thick cross-bedded units of restricted lateral extent (up to 10 m wide). The thin matrix-supported cross-bedded conglomerates horizons are discontinuous and laterally pass into fine-grained sandstones and siltstones.

Interpretation - The coarse sediments and lenticular shape of these units suggest that this facies corresponds to the development of small channels.

3.2.2.3 Facies association interpretations

3.2.2.3.1 FA3: Alluvial fan (LFAT1-3)

The vertical profile of the stratigraphic units, with low-relief erosion surfaces at the base of the two first conglomerates, the presence of small lenses of matrix-supported conglomerates, overlain by trough cross-bedded coarse sandstones, and followed by planar medium to fine sandstones indicate a rapid decrease in flow competence and is characteristic of sheetflood deposits (Kerr, 1984). The cross-bedded sandstone lenses deposited by waning flow as floodwaters declined (Bluck, 1967; Heward, 1978) indicate a rapid streamflow attenuation, which is characteristic of alluvial fan deposits (Nilsen, 1882; Blair and McPherson, 1994). The non-erosive, unstratified conglomerates are deposited by laminar gravity flows and form debris flow deposits building clast-rich lobes (Blair and McPherson, 2009). Larger lobe deposits are more common in the distal part of an alluvial fan deposits (Miall, 1977; Blair and McPherson, 1994).

The homogeneous pale purple-pink outcrop colour suggests subaerial oxidising conditions. The finer-grained sheet-like sandstones with rare paleosols (LFAT3), separating the different conglomerate and sandstone units, reflect overbank flow deposits, potentially homogenized by root activity.

FA4: Braided river (LFAT4-6)

The fining-upward conglomerates and sandstones are interpreted to represent cyclic channel deposits in a braided river environment (Williams and Rust, 1969; Miall, 1977, 1996; Bridge, 2003). The erosive clast-supported conglomerates with horizontal stratification were deposited by bar migration (Rust, 1972). The presence of interbedded sandstones lenticular beds indicates a compound braid bar system. The planar and low angle cross-stratified conglomerates are typical of the initial deposition of mid-channel bars dominated by bedload transport (Bridge, 1993; Lunt and Bridge, 2004). These bars are formed by migration of gravel sheets downstream and can later be cut by second order cross-bar channels. The interbedded sandstones and presence of aligned pebbles are the result of ephemeral conditions (waning flow) or secondary transverse flows (Rust, 1972, 1978; Bridge, 1993). Sandy deposits were concentrated in topographically high parts of the channel belt and in channel fill during the falling stage of floods.

3.2.2.3.2 FA5: Flood plain (LFAT5-7)

The mudstones and siltstones interbedded with minor sandstones are interpreted to represent floodplains in inter-fluve areas. This association of facies can be encountered in overbank deposits or result from waning flood (Miall, 1977). Sandstones fining upward to siltstones and mudstones, and heterolithic facies such as flaser bedding can be encountered in mud-dominated flood plain deposits (McCarthy et al., 1997). The association of well-sorted fine sand and silt with climbing ripples and cross-lamination represents multiple fining-upward episodic depositional events. These have been interpreted as overbank crevasse-splay deposits, where variations in grain sorting can be related to the differences in sediment load depending on the water discharge (Lunt and Bridge 2004). The small channels formed by the matrix-supported conglomerates (LFAT10) are here interpreted as crevasse channels bringing sediments to the unconfined flood plain (Miall, 2006; Burns et al., 2017). This facies association therefore reflects flood plain deposits (Smith 1980).

3.2.3 Transitional environments

Transitional environments have been observed between the fluvial Amsittène Fm and the marine Tamarout Fm. They have been attributed to the upper part of the Amsittène Fm for a better recognition in the field as they present a dominant red colour characteristic ofcontinental deposits.

3.2.3.1 Depositional architecture

3.2.3.1.1 Tizgui

Above the alluvial deposits (FA4 and FA5) of Tizgui, a mixed carbonate and siliciclastic unit developed (Fig. 10). It is mainly composed of mudstone and marls (LFTR1) alternating with siltstones (LFTR2), dolomitic sandstones (LFTR3) and sandy dolomite (LFTR4) (Fig. 10). The lower part of this unit is dominated by red mudstones and interbedded dolomitic sandstones and siltstones. Up-section the unit is dominated by sandy and silty dolomite, alternating with marls and mudstone horizons.

3.2.3.1.2 Tikki

Twelve meters of red mudstones and siltstones with horizons of nodular gypsum are developed around Tikki (Fig. 10). At the top of this unit, sandy dolomite levels (LFTR4), sandstones and siltstone horizons (LFTR6) appear, still alternating with mudstone (LFTR1) and evaporites (LFTR5). The amount of evaporites decreases towards the top of the unit, which is capped by one meter of wavy-bedded peloidal packstone.

3.2.3.2 Lithofacies LFTR

3.2.3.2.1 LFTR1

Description. - Lithofacies LFAT1 is composed of red and green siliciclastic mudstones and marls (Fig. 10, LFTR1). The units are friable, with no visible sedimentological features. The red to green color transition is parallel to the bedding.

Interpretation - Red and green mudstones and marls indicate deposition in a very quiet, low-energy environment. The red and green colour changes indicate geochemical variations in the groundwater table, and reflect oxidizing and reducing conditions, respectively (Wilson et al., 2014).

3.2.3.2.2 LFTR2

Description - Lithofacies LFTR2 is composed of red siltstones with some mud rip-up clasts at the base, current ripples and locally root traces at the top (Fig. 10, LFTR2).

Interpretation - The rip-up clasts at the base of the beds indicate an increase of energy in the flow regime. The presence of root traces at the top of these beds suggests repeated exposure, which allowed the development of paleosoils.

3.2.3.2.3 LFTR3

Description - Lithofacies LFTR3 is composed of dolomitic sandstones with planar laminations, wave ripples, as well as more massive beds (Fig.10, LFTR3). Some quartz grains present a thin carbonate coating, and occasional carbonate clasts are visible.

Interpretation - The presence of carbonate microspar and carbonate coating could be diagenetic or indicate deposition in a carbonate-rich environment such as a lake or a marine environment. The waves ripples are indicating of bidirectional currents.

3.2.3.2.4 LFTR4

Description - The sandy dolomites contain carbonate-coated quartz grains and some ooids, and feature flaser bedding and wavy bedding with bi-directional flow indications and tabular cross-bedding (Fig.10, LFTR4).

Interpretation - The presence of ooids and carbonate cement indicate the deposition in a water body with some energy. The bidirectional flow indications indicate tidally-influenced facies with sandstones deposited during high-energy periods and mud deposited from suspension at times of slack water.

3.2.3.2.5 LFTR5

Description - Lithofacies LFTR5 is characterised by thins horizons of nodular gypsum beds.

Interpretation - Gypsum nodules are commonly growing from evaporation of hypersaline, sulphate-saturated interstitial waters by displacement of unconsolidated sediments (Murray, 1964; West et al., 1979).

3.2.3.2.6 LFTR6

Description - Lithofacies LFTR6 is composed of thin beds of siltstones and very fine sandstones. These are consolidated by a carbonate cement.

Interpretation - These very thin beds indicate periodic deposition of coarser material. They are characteristic of repeated flooding events.

3.2.3.3 FA6: Coastal plain (LTFR1 and LFTR4-6)

The common mudstone deposits (LFTR1) indicate an overall low-energy environment, while the dolomitic sandstones (LFTR3) with tabular cross-bedding reflect an increase of energy in the environment and currents eroding the underlying deposits. The increase in sandy dolomites (LFTR4) towards the top of the unit suggests a change in the environment of deposition as the formation of ooids and coated grains requires marine or lacustrine conditions. These sandy and silty dolomites are likely to be marine intercalations, but a potential lacustrine origin cannot be discounted. Abundant flaser bedding with ripples indicating opposing flow directions in facies LFTR4 suggests tidal influence. Facies FA6 is dominated by continental deposits (LFTR1, LFTR2), with occasional development of shallow water bodies, which could be lacustrine and/or marine incursions (LFTR3, LFTR4). It records the transition to the overlying shallow-marine Tamarout Fm and it is interpreted as a coastal plain facies association.

3.2.3.4 FA7: Sabkha

The discontinuous appearance of the evaporite (LFTR5) levels in a silty-clay (LFTR1) matrix can be explained by gypsum crystals growing in the capillary zone and displacing silts and clay as they grow (Warren, 1991). The sandstones and siltstones (LFTR4 and LFTR6) indicate a minor but consistent siliciclastic influx. The presence of evaporites, the marine indications, and the transitional position between the continental Amsittène Fm and the shallow marine deposits of the Tamarout Fm suggest a coastal character for this evaporitic environment. It was likely a coastal sabkha, potentially linked with shallow groundwater resurgence or supratidal water flooding.

3.2.4 Tamarout Formation

The upper part of the Tamarout Fm in Tikki, and the entire formation in the western part of the basin contain interbedded dolomites, marls and limestones (Fig. 11 and 12) (Adams et al., 1980). Brachiopods reported by (Ambroggi, 1963) and fragments of echinoderm observed in thin sections are evidence for an overall open marine environment. In the East and North of the basin these facies alternate with extensive evaporites (LFTA9a), while in the South and West of the basin the evaporites disappear and are replaced by upwards thickening breccia units (LFTA9b).

3.2.4.1 Depositional architecture

Following locally either the sabkha or coastal plain environments, the Tamarout Fm is characterised by the transition to tidal limestones. Three different units have been distinguished according to facies proportions and stratigraphic organisation (Fig. 13). Unit T1 at the base of the formation is dominated by laminated dolomite, cross-laminated peloidal and oolitic grainstones and minor bioclastic PST and inversely graded breccias. Overlying unit T2 consists of thin dark stromatolite horizons, meter-thick breccia, cross-laminated oolitic and peloidal PST and GST and thinly-bedded dolomite. Unit T3 consists of interbedded yellow crystalline and sandy dolomite with dark grey oolitic PST and GST, rare breccias with centimetre to decimetre-large clasts and grey marls.

3.2.4.2 Lithofacies interpretation

3.2.4.2.1 LFTA1

Description - Lithofacies LFTA1 consists of centimetre to meter-thick dolomite beds. It is dominated by euhedral and anhedral dolomite crystals, with rare shell fragments and some quartz-rich horizons. Sedimentary features include cross-bedding, cross-laminations and heavily bioturbated horizons (Fig.11, LFTA1).

Interpretation - Dolomitisation affected variable depositional textures; preserved cross bedding indicates that some formed under relatively high energy levels. The dolomite horizons formed by reflux of low temperature dolomitizing fluids (Al-Sinawi et al., 2017). This process is often associated with peritidal carbonates and evaporites (Lu and Meyers, 1998; Flügel, 2010), and is consistent with the presence of stromatolites and evaporites elsewhere in this formation (see below).

3.2.4.2.2 LFTA2

Description - Lithofacies LFTA2 consists of bioclastic wackstones and packstones. (Fig. 11, LFTA2; Fig. 12, a). The bioclastic elements are unbroken or large fragments of brachiopods, bivalves and gastropods, organised in horizontal beds in a muddy matrix.

Interpretations - The muddy matrix indicates a relatively low-energy while the good sorting of the bioclasts indicate a higher energy environment. This facies can be attributed to subtidal environments where reworked bioclasts can be brought in by tidal currents and form lag horizons (Flügel, 2010).

3.2.4.2.3 LFTA3

Description - Peloidal and oolitic wackstones and packstones make up LFTA3. Occasional bioclasts are present, and the amount of fine quartz grains is very variable. Common heterolithic stratification (Fig. 11, LFTA3; Fig. 12, b) displays wavy bedding and flaser bedding, with sharp contacts at the base of the oolitic or peloidal horizons, and more gradational disappearance of the wave ripple elements in the muddy matrix. Locally the sorting of the ooids and the sand is very good and the muddy matrix is replaced by dolomitic sparite.

Interpretations - The wavy and flaser bedding are evidence for variations in the flow intensity. While the ooids need some energy to form, the peloids require less energy to be preserved and mud is deposited in a very low energy environment. The sharp contact at the base of the oolitic-streaked and peloidal-streaked muds and more gradational top likely reflects variable current flow velocity. Stronger tidal currents bring in the oolitic or peloidal grains, whereas the subordinate tidal current will be depositing the mud in the system. These heterolithic stratifications are characteristic of an intertidal environment (Flügel, 2010). Local good sorting of the elements indicates a consistent flow, and the disappearance of the mud is diagnostic for higher-energy tidal currents.

3.2.4.2.4 LFTA4

Description - Lithofacies LFTA4 is composed of peloidal packstones and grainstones with <40% quartz of uniform grain size. Cross-stratification, cross-laminations, waves ripples and herringbone cross-stratifications are common (Fig. 11, LFTA4; Fig. 12, c). The siliciclastic elements are fine to very fine, sub-angular to sub-rounded quartz grains associated with low-angle cross-bedding and wave ripples.The same sedimentary structures are observable weither quartz grains are present or not.

Interpretation - The large proportion of very well sorted sand and the presence of herringbone cross-stratifications in the peloidal GST are evidence for reworking by bidirectional currents in an intertidal environment. The mixed (peloids and sand) wave ripples are indicative of important reworking of elements originating from different sources. This lithofacies is interpreted to record inter-tidal to sub-tidal environments where oscillatory currents are common.

3.2.4.2.5 LFTA5

Description - Lithofacies LFTA5 contains various oolitic grainstones(Fig. 11, LFTA5; Fig. 12, d, e). Tangential ooids are common, often partly overprinted by micritization. In the upper part of the succession, the oolitic grainstones are composed of compound ooids and single ooids with radial-concentric fabric surrounded by tangential-concentric microfabric. The nuclei of the ooids are variable, often fine quartz grains or bioclasts. Sedimentary features include swaley cross-stratification, horizontal laminations and wave ripples (Fig. 11).

Interpretation - Tangential ooids are associated with very shallow water in high energy setting and hypersaline environment (Davies et al., 1978). The radial ooids can form in marine setting as well as in saline and fresh-water lakes, and the transition to tangential concentric fabric reflects a change of water energy to a more agitated environment (Tucker, 2009; Flügel, 2010). The good sorting of the ooids and their various nuclei associated to planar cross-bedding are reflecting high energy marine environments, most likely oolitic shoals or tidal bars. The presence of swaley cross-stratification in the oolitic GST demonstrates higher energy storm-wave currents, which are often developed in slightly deeper peritidal settings.

3.2.4.2.6 LFTA6 and LFTA7

Description - Lithofacies LFAT6 is dominated by carbonate mudstones with sparse carbonate mudstone clasts and occasional bioturbation (Fig. 11, LFAT6). Lithofacies LFAT7 is composed of green and grey marls in centimetre thick units (Fig. 11, LFAT7). The difference between these two lithofacies derives from the higher clay content in LFTA7.

Interpretation - The mudstone and marl horizons (Fig. 11, LFTA6 and LFTA7) formed in very low-energy environments, with some influx of clay material. Mudstones locally broken into mudstones pebbles are associated to supratidal environments (Strasser, 1988).

3.2.4.2.7 LFTA8

Description - Lithofacies LFAT8 is composed of dark micritic horizons of stromatolites. The stromatolites observed are stratiform, thinly laminated irregular microbial mats with a strong kerogenic smell (Fig. 11, LFAT8)

Interpretation - The stromatolites (Fig. 11, LFTA8; Fig. 12, f) are stratiform microbial carbonates, which develop in very low-energy, upper intertidal to supratidal environments (Hoffman, 1976; Beukes et al., 1989; Tucker, 2009).

3.2.4.2.8 LFTA9

Description - Lithofacies LFAT9a and LFAT9b has been grouped together as they are interpreted to be genetically related. They consist of continuous and lenticular gypsum and breccias beds between a few centimetres and several meters thick (Fig. 13). Lithofacies LFTA9a is composed of gypsum beds, mostly massive, with some rippled micritic carbonate horizons (Fig. 11, LFAT9a; Fig. 12, g). In the breccia horizons (Fig. 11, LFTA9b), angular clasts are inversely-graded and degree of brecciation decreases to the top of each bed, with tops commonly only consisting of crackle breccias, where clasts are still in place but separated by calcite veins (Fig. 15, A). The clast lithology matches the surrounding host sediments (laminated dolomite, oolitic GST and stromatolites). These two facies are commonly associated to dolomite levels and microbial laminated horizons (LFTA8).

Interpretation - The lateral continuity of some evaporites horizons and their association to centimetre-thick, microbial-laminated carbonates and dolomite levels indicates temporarily subaqueous conditions (Rouchy and Caruso, 2006; Warren, 2016). To develop extensive evaporitic levels, the environment must be very restricted, with little influx of waters of lower salinity. The inverse grading, variable lateral extension, absence of preferential orientation of the clasts in the breccias beds, and the absence of breccias where the evaporites are intact, are evidence for a collapse-dissolution origin of the breccias (Friedman, 1997). Collapse occurred after deposition when evaporite beds came in contact with under-saturated fluids, such as meteoric water or seawater of lower salinity (Warren, 2016).

3.2.4.3 Facies association interpretations

3.2.4.3.1 FA8: Subtidal to intertidal carbonates

This facies association is characteristic of the units T1 and T3 (Fig. 14). The association of minor marl horizons with dm-thick oolitic PST, oolitic grainstones and abundant dolomite beds is a sign of reworking of the fine-grained material in relatively low-energy settings. The lithofacies range from common intertidal peloidal GST and dolomite to subtidal oolitic GST and bioclastic GST. The disappearance of stromatolites in unit T1 and T3 indicates an opening of the environment of deposition. Dissolution-collapse breccias only appear at the top of unit T1 and at the base of unit T3, and mark the transition from the intertidal to subtidal environment (T1 and T3) to a more restricted environment (T2). The overall environment of deposition is interpreted as subtidal to intertidal.

3.2.4.3.2 FA9: Supratidal carbonates

This facies association is characteristic of the unit T2 (Fig. 14), and is organised in shallowing-upward peritidal cycles (Fig. 15). Cycles consist of intertidal dolostone (LFTA1), followed by sharp-based peloidal and oolitic PST and GST (LFTA3, LFTA4 and LFTA5) which might represent a transgressive phase (Strasser, 1988). The inter to supratidal stromatolites (LFTA8) and evaporites (LFTA9a), often replaced by dissolution breccias (LFTA9b), indicate restriction in the environment and supratidal conditions. Such cycles are characteristic of sabkhas or small coastal salinas in a broad saline tidal flat environment (Friedman, 1997; Warren, 2016).

3.2.5 Ameskhoud Formation

The Ameskhoud Fm shows facies variation across the basin and is here described from the location of Assif El Hade, where it is 240 m thick (Fig. 2). This location is situated in the middle of the basin and records characteristics transitional between the two end-member facies observed (fluvial-dominated in Tikki and Askouti; shallow-marine carbonates in the Amsittène Anticline).

3.2.5.1 Depositional architecture

At Assif El Hade the Ameskhoud Fm can be divided into two units, both dominated by siliciclastic deposits. It overlies the oolitic Unit T3 of the Tamarout Fm, which shows an increasing proportion of quartz grains, up to 20-40%. The very base of the Ameskhoud Fm is composed of sandy and silty dolomite alternating with red clay and marls (Fig. 17, a). The siliciclastic fraction of the sediment increases rapidly up-section and well-sorted dolomitic siltstones and very fine- to fine-grained sandstones become dominant. Facies developed in the lower part of the formation include red mudstones (Fig.16, LFAK1), siltstones and fine to coarse sandstones (Fig. 16, LFAK2 and LFAK3).

The upper part of the formation is composed of thick, red mudstone (Fig. 16, LFAK1) units with intercalations of silt and sandstone beds (Fig. 16, LFAK2,LFAK4 and LFAK5) and rare nodular carbonate horizons.

3.2.5.2 Lithofacies

3.2.5.2.1 LFAK1

Description - Lithofacies LFAK1 is composed of massive and bedded red mudstones, with occasional beds of carbonate nodules (Fig. 16, LFKA1), which are only present in the upper part of the formation. They are very vuggy and often form calcite geodes (Fig. 17, a and b).

Interpretation - The very fine-grained material was probably deposited in a low-energy environment. The red color indicates oxydizing conditions or transported oxydized material. The carbonate geodes are a diagenetic feature, often formed during early phases of compaction, which might have formed from the dissolution of evaporites nodules (Tucker, 2003) or by preferential pore-water movements (Tucker, 2001).

3.2.5.2.2 LFAK2

Description - Lithofacies LFAK2 is composed of siltstones and sandstones, displaying (Fig. 17, b), horizontal and low angle cross-bedding and wave-ripples. The thickness of the siltstone units varies from a few centimetres up to 10 meters.

Interpretation - The wave ripples indicate oscillatory currents, and the relatively good sorting of the material indicate some reworking.

3.2.5.2.3 LFAK3

Description - Lithofacies FFAK3 is acorresponds to very fine to very coarse grained, well to moderately sorted sandstones. Some beds are extensively bioturbated. Highly bioturbated beds have an upper surface dominated by *Ophiomorph*a and *Rhizocorallium* (Fig. 17, d), sometimes *Diplocraterion*. Some erosive, irregular beds of coarse to very coarse grained sandstones and non-erosive fine and coarse sandstones become common in the upper part of this unit (Fig. 16, LFAK3). Wave ripples, horizontal parallel lamination and cross-bedding with occasional mud drapes are mostcommon features frequently overprinted by bioturbation.

Interpretation - The presence of *Ophiomorph*a, *Rhizocorallium* and *Diplocraterion* indicates a marine environment (Gerard and Bromley, 2008). Cross-bedding and planar laminations suggest a relatively high energy environment. The mud draped cross-beds are characteristic of tidally influenced environments.

3.2.5.2.4 LFAK4

Description - These sandstones are fine- to coarse-grained, well- to poorly-sorted and display horizontal and cross-bedding and current ripples (LFAK4). Some of the medium- and coarse-grained sandstones have an erosive base and a lenticular shape, whereas others present flat top and base. These erosive beds fine-upwards, containing red clay mud-clasts and locally some angular quartz granules just above erosive surfaces (Fig. 17, e), followed up section by planar and trough cross-bedding, with mud-clasts still present. The upper part of the beds is generally bioturbated or contains current-ripples and occasional ripple-drift cross-lamination.

Interpretation - The erosive fining-upward, lenticular beds with cross-beds and current ripples have been interpreted as minor channel deposits. The cross-sets in sandstones are developed oblique to the channel axis, representing lateral accretion (Allen, 1963), while the ripple-drift cross lamination are interpreted as the product of waning flows in the transition to suspension mudrocks (Nanson, 1980).

3.2.5.2.5 LFAK5

Description - This lithofacies comprises more extensive beds of very fine- to medium-grained sandstones (LMAK5) with thin horizontal-bedding and cross-bedding have sharp, but non erosive bases (Fig. 17, f). Some of these beds are also bioturbated and display roots traces (Fig. 17, g). Beds with good sorting display horizontal bedding, trough cross-bedding and ripple laminations, with occasional mud drapes between the cross-beds and bidirectional currents. Some of these beds are heavily bioturbated, the most common trace fossil being *Thalassinoides* and *Arenicolites* (Fig. 17, h) on top of the beds. All individual sandstones beds are quite thin (up to 50 cm thick) while the clay horizons can be up to 5m thick.

Interpretation - The root traces are evidence for paleosols and imply exposure.

The association of *Thalassinoides* and *Arenicolites* indicate a marine environment. The trough cross-bedding indicates a high energy environment. The root traces are evidence for paleosols and imply exposure. These are interpreted to be possible crevasse or sheet sandstones.

3.2.5.3 Facies associations interpretations

3.2.5.3.1 FA10: Near shore siliciclastics

The sandy and silty dolomites at the base of the Ameskhoud Fm were deposited in a similar environment to the upper part of the Tamarout Fm, but the alternation with red mudstones indicates an increase in terrestrial influx. The well-sorted siliciclastics with oscillatory currents and *Ophiomorpha* are interpreted as a high-energy nearshore sequence (Howard and Reineck, 1981; Goldring and Bridges, 1973; Droser and Bottjer, 1989; Knaust, 2013). Facies architecture and the general coarsening upward of the succession, followed by tidal flat deposits, indicates a progradation (Tucker, 2001). These nearshore siliciclastics represent tidally-influenced shallow marine shelf sediments deposited on top of the relief inherited from the Lower Jurassic carbonate shelf.

3.2.5.3.2 Intertidal to supratidal siliciclastics

The dominance of red mudstones in the upper part of the Ameskhoud Fm indicates a low energy environment. The presence of isolated small channels, always separated by mud horizons (Fig. 17, e), are interpreted as avulsing small tidal channels. The mud-dominated deposits with carbonate nodules and palaeosols formed on a floodplain/tidal flat, subjected to ephemeral floods, which deposited ripple and horizontal-bedded sandstones (Turnbridge 1984, Muñoz et al., 1992). In the sandstones units, occasional bidirectional currents and mud drapes between the cross beds indicate a tidal influence (Boersma & Terwindt, 1981). The repeated successions of trough cross-bedding, cross-beds and ripple laminated sandstones, encased within mudstones and siltstones, indicate variations in currents strength, which could result from the migration of small tidal channels and sand waves (Tucker, 2001). The association of well-sorted sandstones with *Thalassinoides* and *Arenicolites* trace fossils is also characteristic of tidal flat deposits (Gerard and Bromley, 2008). The upper part of the Ameskhoud Fm at Assif El Hade therefore represents intertidal (tidal flat) and supratidal (tidal marsh, ephemeral channels) deposits (Terwindt, 1988).

3.2.6 Regional variations

Southern EAB

To the south and east of the basin, in the locality of Askouti and Tikki (Fig. 2), the Ameskhoud Fm is thinner (100 m). No tidal influence can be observed and the succession contains massive and horizontally-bedded red mudstones and siltstones interbedded with sandstones and lenticular conglomerates. The conglomerate beds are erosive, crudely-bedded and tabular cross-stratified. They often form part of fining-upward units and are topped by cross-bedded and horizontally-bedded sandstones. The red mudstones and siltstones locally form successions up to 8m thick and display abundant root traces. The sandstones or conglomerates can be interpreted as alluvial / fluvial deposits; braided bar or channel lags (Rust, 1972; Nemec and Postma, 1993; Lunt and Bridge, 2004). The mud- and silt-dominated facies, laterally associated to these fluvial channels, are interpreted as overbank / flood plain deposits.

In the location of Askouti, decimeter-thick evaporite horizons are present that progressively disappear towards the top. In this location, this formation also contains continental deposits interbedded with playa evaporitic deposits. The gypsum beds indicate an arid environment that was occasionally flooded and dried out. These deposits present characteristics of playa lake evolving to fluvial deposits (Handford, 1982).

3.2.7 Northern EAB

Along the Amsittène anticline and in the wells ESS-1 and TMS-1 (Fig. 2), the Middle Jurassic deposits display a very different character from the rest of the basin. This interval is composed of dolomite beds alternating with oolitic grainstones, some anhydrite and gypsum horizons, and some grey and red marls horizons. The facies of these wells and outcrops are very similar to the facies described in the Units T1 and T2 of the Tamarout Formation. The presence of red marls and evaporites can be linked to coastal salina deposits and the oolitic and dolomitic beds are interpreted as peritidal to subtidal deposits.

4 Basin evolution

4.1 Regional correlations

Variation of facies and lateral extent of the sedimentary sequences is illustrated using 5 sections (Fig. 19, locations B, C, D, E and F). The Essaouira-1 (ESS1) well (Fig. 19, location A) constrains the extent and character of the Arich Ouzla Formation, that otherwise only outcrops in the core of the Amsittène Anticline (Fig. 2).

The nomenclature used is derived from Depositional Sequence IV described by Catuneanu et al (2009, 2011), based on Hunt and Tucker (1992, 1995) and Helland-Hansen and Gjelberg (1994). The observation and interpretation including lateral and vertical facies organisation and variability, unconformities and correlative conformities and geometries of the units, enabled the identification of parasequences. General transgressive and regressive trends were identified and correlated across the basin in order to build a coherent framework for the Lower and Middle Jurassic deposits.

4.1.1 Chronostratigraphic constraints

4.1.1.1 Sinemurian-Pliensbachian

The first datable correlation surface of the sections is the top of the CAMP basalts, which were emplaced in Morocco around 199 Ma (Marzoli et al., 1999; Knight at al., 2004; Nomade et al., 2007; Davies et al., 2017). Biostratigraphic markers are sparse in the Arich-

Ouzla Formation, but available fauna is dated as Late Sinnemurian to Early Pliensbachian (Peybernes et al., 1987; Du Dresnay; 1988). The equivalent level in the DSDP borehole 547B (leg 79; Bernoulli and Kälin, 1984; Riegraf et al., 1984) is also dated as Late Sinemurian to Early Pliensbachian.

4.1.1.2 Toarcian

Based on the marked lithological change, erosion and age relationships of underlying and overlying units, the unconformity at the base of the Amsittène Formation is correlated to the base of the Azilal Formation in the Central High Atlas, where it has been dated as lower Toarcian (Lachkar, 2000; Wilmsen and Neuweiler, 2008; Malaval, 2016). The Toarcian age of the Tamarout Formation (Ambroggi 1963; Peybernes et al. 1987) is based on brachiopod identification, including *Terebratula withakeri* (Oppel) and *Zeilleria anglica* (Walker), and supported by identification of the Dasyclad *Sarfatiella dubari* in the Essaouira Basin (Bouaouda, 1987).

4.1.1.3 Middle Jurassic

For the Ameskhoud Formation, only relative dating and superposition is available to define the formation age. Dating by foraminifera assemblages gives an Upper Bathonian age for the base of the overlying Ouanamane Formation (Bouaouda, 1987, 2004, 2007). The underlying Amsittène Formation, being dated Toarcian, gives an bracketed aged for the Ameskhoud Formation of Aalenian to Bajocian/Bathonian (Bouaouda, 2004).

4.1.2 Sequence Stratigraphy

4.1.2.1 Sinemurian-Pliensbachian – Sequence 1

The Arich Ouzla Formation was deposited on Triassic red mudstones. These deposits mark the last fully continental deposits before the onset of carbonate platform development (Fig. 19, A and B). The marine flooding surface at the base of the Arich Ouzla Formation is recognised as the first transgressive surface and can be correlated between the Arich Ouzla section and the well ESS-1 (Fig. 19). The transition from lagoonal deposits (Fig. 5, FA1) to middle ramp deposits (Fig. 5, FA2) records an important transgression. Later, smaller oncoid and coral fragments record higher energy environments, with marks the beginning of a regression. In the locality of Amsittène, the last crinoids-rich bed before appearance of coral fragments are associated with a diminution of oncoid size, considered as a the top of the Transgressive System Tract. This transition of depositional trend from retrogradation to progradation defines the first Maximum Flooding Surface (MFS1) (Frazier 1974; Posamentier et al. 1988; Van Wagoner et al. 1988) (MFS1, Fig.19).

4.1.2.2 Toarcian – Sequence 2

The base of the Amsittène Formation is defined by a strong erosion surface, cutting down in places to the CAMP basalts (Tizgui, Fig. 2) or the Triassic continental reed beds (Imi N'Tanoute, Imi'N Trili, Fig. 2) in the Agadir sub-basin, and cutting into the upper part of the Arich Ouzla Formation along the Amsittène Anticline (Fig.19, B). In this location, the upper part of the Sinemurian is also marked by karstification and the contact to the Amsittène Formation is an angular unconformity, carving through the dolomites and filled by dolomitic and sandy breccias (see section 3.2.4). This contact is interpreted as a subaerial unconformity, with eveience for fluvial erosion, pedogenesis or karstification, and thus marks a period of relative base-level fall (Posamentier et al., 1988; Aitken and Flint, 1996; Plint and Nummedal 2000) and is defined as a Sequence Boundary (SB2) (Hunt and Tucker, 1992). This sequence Boundary SB1 can be traced over the basin (Fig. 19). In well ESS-1 its correlative conformity is marked by the abrupt transition from carbonate deposits to siliciclastics.

Above SB2, a transgressive succession from flood plain to coastal plain deposits of the Amsittène Formation, is followed by sabkha deposits near Essaouira. This transgression continues with deposition of the shallow-marine Tamarout Formation. The first marine deposits form the upper part of a transgressive system tract. The dolomitic, peloidal and bioclastic succession at the base of this formation records an intertidal to subtidal environment. The maximum flooding surface MFS2 has been defined as the first appearance of subtidal grainstones in all the locations, which records the most open marine deposition of this formation. The intertidal and subtidal succession (Fig.14, Unit T1) following MFS2 records shallower deposits forming a regressive package (Fig.14, Unit T2). This latter package is dominated by peritidal cycles where stromatolites and dissolution breccias or evaporites constitute the more proximal deposits. A fourth order sequence boundary SB2-1 is defined by the appearance of the first peri- to supratidal cycle capped by thick (10m) dissolution breccias. SB2.1 is followed by local aggradation leading to deposition of thick (>100m) supratidal carbonates identified as a low stand system tract. The following deposits suggest deeper conditions again, with a transition from mainly supratidal to mainly peritidal and subtidal deposits in the upper part of the Tamarout Formation. The top of the first extensive oolitic grainstones after the last occurrence of dissolution breccia marks the return to a higher energy environment and can be identified as a fourth-order maximum flooding surface (MFS2.1). This is followed by the development of a second succession dominated by subtidal deposits characterizing a highstand system tract.

The overlying Ameskhoud Formation records a strong regression in the south of the basin with development of fluvial deposits (Fig. 19, E and F), while the equivalent levels in the north of the basin only record supratidal deposits (Fig. 19, B and C). . The initial fluvial erosion in the locality F records an unconformity which defines sequence boundary SB3. It is represented by its correlative conformity marked by shallow marine deposits and the first major influx of siliciclastics in the carbonate-dominated succession of the Essaouira Basin (Fig. 19, B) and by the first supratidal deposits in the locality of Assif El Hade (Fig. 19,C). The following peritidal to supratidal sequence of the Ameskhoud Formation in the North (Fig. 19, C) and playa lake to fluvial in the South (Fig. 19, E and F) form a lowstand system tract.

4.1.2.3 Middle Jurassic – Sequence 3

Towards the upper part of the Ameskhoud Formation, a wedge of peritidal deposits (Fig. 19, C) record a small transgression associated to a fourth order maximum flooding surface MFS3.1. In the Essaouira Basin, the expression of the MFS3.1 is linked to the transition from coastal plain or marly deposits to carbonate-dominated marine deposits (Fig. 19, B). The upper part of the Ameskhoud Formation presents the last regression in the Agadir Basin before returning to fully marine conditions during the Late Middle Jurassic (Ambroggi, 1963; Bouaouda, 1987).

4.2 Paleogeographic interpretations

The evolution of the EAB during the Lower and Middle Jurassic can be sub-divided in four main stages. The transitions between each stage correspond to major shifts in sedimentation between carbonates and siliciclastics.

The Arich Ouzla Formation is dominated by open marine carbonate. It initially records lagoonal and upper ramp carbonates (Fig. 5, FA1), before shifting to more open conditions with midramp facies association (Fig. 5, FA2). Outcrops of this formation are limited in the western part of the Jbel Amsittène, therefore only one section has been studied and the regional understanding of extent and pattern of this depositional environment interpretion is limited.

The continental deposits of the Amsittène Formation consist of facies associations FA3, FA4, FA5 (Fig. 7), interpreted as alluvial fan to flood plain deposits (FA3 to FA5).In the Agadir sub-basin, the more proximal deposits are composed of braided river, flood plain and alluvial fan deposits. In the area of Tikki, the Amsittène Formation evolves vertically from a flood plain to alluvial fan deposits. This alluvial fan probably relates to activity along an ENE-WSW trending fault, parallel to the major Tizi N'Test fault (Laville and Petit, 1984; Hafid et al., 2000; Frizon de Lamotte et al., 2009) which can be traced from the Argana Valley to the Northeast of the Imouzzer Anticline (Fig. 2). This fault might be linked to the western termination of a Lower to Middle Liassic rifting phase of the Atlas Tethys (Frizon de Lamotte et al., 2009). Erosion of the footwall would have sourced the local alluvial fans in Tikki, while most of the sand-grade deposits in the Agadir Basin probably came from the erosion of older highs further afield, such as the Western Meseta and the Rehamna (Fig. 18, A).

The vertical succession of floodplain to coastal plain deposits in the upper part of the Amsittène Formation records a transgression, ultimately leading to the shallow marine deposits of the Tamarout Formation. Units T1 and T3 of the Tamarout Formation record shallow-marine, open-ramp, oolitic and bioclastic WST to GST all over the basin, with local oolitic shoals (Fig. 18, B1, FA8). Sabkha and coastal plain deposits can be identified behind the shoreline (FA5), disconnected from the platform, but receiving episodic to periodic marine incursions. The widespread development of evaporites, stromatolites and dissolution breccias in unit T2 reflects a more restricted environment with hypersaline conditions (Fig. 18, B2, FA9). During restricted periods, sabkha or coastal salinas developed in a large saline tidal flat. Marine ingressions led to a more open-marine system with development of higher energy facies.

The presence of siliciclastic deposits in the Tamarout Formation can be linked to a river system entering the Essaouira-Agadir Basin, sourced from uplifting massifs to the east. Red sandstones can be identified, often associated with evaporites (Fig. 18, B1).

The overlying Ameskhoud Formation is strongly regressive. In the southeast of the basin, continental facies are dominating, and an important alluvial plain with braided rivers (FA2, FA3) is developed in Tikki and Tizgui (Fig.18, C). In Askouti, a similar facies is observed, with intercalations of decimetre-thick evaporite beds (FA5) which are characteristic of playa lake deposits (Fig. 18, C). The locality of Assif El Hade records basal unit composed of subtidal to intertidal siliciclastic deposits (Fig 16, Fig. 18, FA10) that grade upward to intertidal to supratidal with occasional continental flood plain deposits (Fig. 16, Fig. 18, FA11). These siliciclastic deposits contrast sharply with the restricted marine carbonate dominated sediments preserved at the same period in the Essaouira sub-basin (Fig. 18, C, FA8 and FA9).

5 Discussion

Following the end of rifting, Lower Jurassic deposits in the EAB record an initial marine incursion in the Central Atlantic basin. A marine carbonate ramp developed during the Sinemurian-Pliensbachian (Arich Ouzla Fm and DSDP 547B leg 79 basinal equivalent) in the western and northern portions of the basin. The absence of Sinemurian-Pliensbachian deposits further east and south suggests that either the earliest Jurassic marine incursion(s) did not reach these parts of the basin, or, more-likely, that any Sinemurian-Pliensbachian deposits were subsequently eroded by the basal Toarcian unconformity. The Toarcian transgression can be linked to the global early Toarcian transgressive event (Fig. 19; Hallam, 1981). Shallow carbonate platform environments were established across the study area in the later Toarcian (Amsittène and Tamarout Fms) and in the Central High Atlas. This was followed by regression in the Toarcian-Aalenian, leading to renewed deposition of the continental Ameskhoud Fm.

5.1 Toarcian erosion

EAB stratigraphy

The contact between the Sinemurian Arich Ouzla Formation and the Amsittène Formation is erosive and locally filled by sandy dolomitic breccias and karstified, which indicates a period of emersion during the Pliensbachian or Early Toarcian (Fig. 19, B). An angular unconformity can be observed that indicates tectonic activity (Fig. 20).

Two different mechanisms can explain these deposits. In the first hypothesis (Fig. 20) emersion and karstification of the upper Arich Ouzla Formation are related to tilting and faulting of the formation. Erosion of the newly created relief delivered angular fragments at the fault toe where they could be reworked with siliciclastic deposits. In an alternative scenario, uplift and folding of the anticline caused erosion and karstification. Both hypotheses require vertical movements within the basin during the Toarcian. This broadly coincides with the timing of erosional exhumation of the Anti-Atlas and massifs of the Meseta (Gouiza et al., 2017 and Ghorbal et al., 2008, respectively). No exhumation study (low-temperature thermochronology) has been carried out in the EAB itself.

An alternative mechanism could be salt mobilisation, which is documented by mini-basin formation at this time in the offshore counterpart of the basin (Pichel et al., 2019). Investigations of exposed anticlines onshore EAB also suggest Early Jurassic vertical movements associated with local salt mobilisation (Kluge, 2016; Charton et al., in prep).

Correlation with the Central High Atlas

The synchronous evolution of the Western High Atlas and the Central High Atlas from the Trias to Middle Jurassic period has been previously suggested in the litterature (Ambroggi, 1963). Comparing the two basins assesses the role of the exhuming massifs (Rehamna, Massif Ancien and Central Anti-Atlas) in the evolution of these two adjacent basins.

The Essaouira-Agadir Basin forms the western termination of the Atlas System and is influenced by the opening Atlantic. Deposits in the Central High Atlas (Saura et al., 2014; Malaval, 2016; Joussiaume, 2016; Moragas et al., 2016, 2017, 2018; Martin-Martin et al., 2017; Teixell et al., 2017, Verges et al., 2017) show affinity to the Tethys. A stratigraphic correlation between the Central High Atlas (CHA) and the Western High Atlas (WHA) allows comparison of regional trends (Fig. 21). In the Central High Atlas, Lower Jurassic deposits are composed of a thick open marine successions. Open platform carbonate sediments of the Bou Imoura Formation were deposited during the Sinemurian and followed by inner platform deposits of the Aganane Formation during the Early Pliensbachian. These deposits are the same age and record similar depositional environments as the Arich Ouzla Formation. This suggests the Central High Atlas and the EAB might have been in communication during this period, connected by an Atlasic sea that allowed exchange between the Tethys and the Atlantic realm. This is consistent with low-temperature thermochronology studies (Ghorbal et al., 2008; Ghorbal 2009; Saddiqi et al., 2009), which interpret the Western Moroccan Arch area as a denuded or subsiding domain during the Late Triassic and Early Jurassic.

At Bin El Ouidane in the CHA (Fig. 21, F), a major Toarcian erosive surface, overlain by continental deposits, cuts down into Pliensbachian (Aganane Formation) inner platform deposits. The Toarcian unconformity recognised in the CHA is interpreted to be coeval with the major erosion surface at the base of the Amsittène Formation (Fig. 21, B, D and E), on the basis of age and lithostratigraphic relationships.

Toarcian siliciclastic deposits recognised in both the EAB and the CHA attest to a widespread erosive event and rejuvenation of the source area(s) during that time. Apatite fission track studies suggest that part of the West Moroccan Arch was exhumed during the Early Jurassic and this is the most likely candidate source area, together with the Anti-Atlas (Ghorbal et al., 2008; Saddiqi et al., 2009, Charton, 2018). The extensive Toarcian erosion, cutting down to the Sinemurian and CAMP basalts, indicates a major regression probably linked to local uplift between the Western and Central High Atlas. The following Toarcian transgression records marine carbonates in the EAB and the CHA (Malaval, 2016; Joussiaume, 2016; Teixell et al., 2017, Verges et al., 2017), which support a regional transgressive event.

5.2 Siliciclastic input: implications and potential provenance

The current study has identified significant siliciclastic input to the EAB throughout the Lower and Middle Jurassic. Potential siliciclastic source areas are the Anti-Atlas and the

Western Meseta (Zaer Massif, Rehamna, Rehamna and Massif Ancien de Marrakech - MAM) (Ghorbal et al., 2008; Charton et al., 2018). Recent compilation work by Charton (2018) records the exhumation of three of the source areas during the Jurassic (Anti-Atlas, MAM and Rehamna), while North of the Meseta, the Zaer Massif and Rehamna were subsiding (Ghorbal et al., 2008). Lower and Middle Jurassic deposits in the Tikki section display paleocurrents towards the W-SW, which also indicates a source from the NE, such as the Rehamna or the MAM. This is consistent with erosion of the West Moroccan Arch during the Toarcian as discussed earlier. The proximity of the source area is also supported by the pebbly to coarse sand grain size and poor overall sorting in the basal Toarcian deposits.

Very strong exhumation rates in the Anti-Atlas during this period (Charton, 2018 after Gouiza et al., 2017) suggest that paleo-relief might have been created, possibly allowing large drainage systems from the Anti-Atlas to extend towards the north / northwest, including into the EAB. There is however, little available evidence to support the re-routing of sediments towards the west. Basalt clasts are found in the Amsittène Formation that may come from basalts within the basin itself at that time, from uplifted fault blocks or basin margin locations. It is however worth noting that the Anti-Atlas also records CAMP activity, with two c.100 km long dykes (e.g. Touil et al., 2008; Silva et al., 2010), that were potentially sourcing basalts to the surface. Thus, the large Variscan belt remains a potential source of sediments for the Toarcian braided river system in the EAB.

In addition to these regional sources, the alluvial fan deposits near Tikki are probably evidence for a local source, linked to activity of this ENE-WSW fault. This fault was subsequently reactivated during the Atlas orogeny and is now a reverse fault, but was probably a normal fault during the Toarcian, with an uplifted footwall to the north. The well-rounded nature of the Toarcian conglomerates in the hanging wall are unlikely to be due to long distance transport, and the preferred interpretation is reworking of older Triassic conglomerates from the footwall (Upper Carnian T6 unit; Mader et al., 2011).

The Tamarout Formation contains a siliciclastic fraction of silt to fine sand delivered into the carbonate-dominated system. Mixed siliciclastic sediments frequently occur in arid settings where there is input of sediments to the nearshore (Belperio et al., 1988; Zonneveld et al., 2001). Siliciclastic sediments in the peritidal environment can be derived from three mechanisms: eolian input, fluvial input or longshore drift (Zonneveld et al., 2001). Sabkha and salina facies are recognised, indicative of an arid or semi-arid climate, under which both ephemeral streams and eolian processes may have operated. Development of coastal eolian dunes is common in arid or semi-arid climate (Semeniuk, 1996) and eolian sand could have been brought into the system by coastal winds, later reworked by the tidal currents and mixed with the carbonates deposits. Only the marine part of the system is observed at outcrop and no eolian or fluvial deposits have been preserved.

During the Middle Jurassic, siliciclastic deposition is only identified in the south of the EAB, while the north of the basin is interpreted to have been too far from the source and still dominated by marine carbonate deposits. This SE (proximal) towards NW (distal) orientation of the system indicates clearly the Anti-Atlas as a potential source. The recorded exhumation of the Anti-Atlas during this period (Charton, 2018) would explain the creation of paleo-relief and the development of an extensive drainage system. The particularly high exhumation rates of the central part of the Anti-Atlas compared to the western part (Gouiza et al., 2017) could also explain the westward direction of flow.

5.3 Middle Jurassic regression

The Middle Jurassic (Tamarout to Ameskhoud formations) displays a transitional evolution from marine carbonate to continental siliciclastics. The base of the Ameskhoud Formation is made of intertidal red siliciclastic deposits, dominated by marls and siltstones interbedded with thick sandstones with cross-stratification and stacked truncated wave ripples. This intertidal facies indicates a change in the composition of the sediments but no relative sea level variation compared to Unit T3 of the underlying Tamarout Formation. Hence, this transition from carbonates to siliciclastics could be decoupled from eustatic change, related to the exhumation of a regional source terrain. This evidence supports the hypothesis first formulated by Stets (1992), and supported by later low-temperature thermochronology studies (Ghorbal et al., 2008; Saddiqi et al., 2009, Charton, 2018) that the West Moroccan Arch (“Terre des Almohades”) was uplifting during this period. The MAM would be the principal potential source for the Middle Jurassic siliciclastic deposits in the EAB.

The regression observable in the EAB during the Middle Jurassic does not correlate with the global eustatic curve (Snedden and Liu, 2011; Haq, 2018). By contrast, the Middle Jurassic deposits are transgressive in the Central High Atlas, where a vast carbonate platform developed until the Bajocian. Siliciclastic deposits were re-established during the upper Bajocian in the CHA (Teixell et al., 2017; Malaval, 2016; Joussiaume, 2016), and during the Bathonian in the Aaiun-Tarfaya Basin, to the South (Arantegui, 2018). This suggests the influx of siliciclastics into the EAB was local, but had to be significant in order to overcome the global Aalenian sea level rise (Haq, 2018; Fig. 19). The regression from intertidal to a continental environment during the Middle Jurassic is interpreted to relate to the tectonic exhumation of the hinterland, resulting in increased sediment delivery to the EAB, and a regression. The absence of siliciclastic deposits in the CHA and Aaiun-Tarfaya Basin can be due to their greater distance to the sediments source in the Anti Atlas.

6 Conclusions

The Early and Middle Jurassic succession of the Essaouira Agadir Basin records the sedimentary response along the passive margin during the opening of the Atlantic Ocean. The succession has also been correlated with equivalent units in the Central High Atlas, to reveal local vs regional depositional trends, and distinguish tectonic from eustatic controls. By identifying the major stratigraphic units and facies of the Western High Atlas and comparing them to the Central High Atlas within a broader framework, this study shows:

1. The oldest Jurassic deposits observed at outcrops in the EAB are open-marine carbonates of the Arich Ouzla Formation. They were uplifted and tilted then partly eroded forming a regional unconformity overlain by continental deposits of the Amsittene Fm during the Toarcian. This unconformity can be correlated across the EAB and to the CHA and records a phase of tectonic uplift of the margin.
2. The Tamarout Formation records a transgression in the upper part of the Toarcian, which led to deposition of intertidal to supratidal carbonates dominated by oolitic limestones, dolomites and evaporites or dissolution

breccias. Three units have been distinguished and linked to variations of the depositional environment, the lateral extent of this carbonate unit and its facies variations on the basin borders have been constrained.

3. The bulk of the Middle Jurassic is marked by a major regression, which led to the establishment of a continental environment to the south of the basin. The input of siliciclastic sediments at this time into the EAB also points towards a tectonic control, with rejuvenation of the hinterland source areas.
4. Lateral facies variations from fluvial deposits to shallow marine carbonates of the Middle Jurassic across the basin have been highlighted and a SE-NW proximal-distal trend has been identified and the siliciclastic origin correlated to the erosional exhumation of the Anti-Atlas.
5. During the Lower and Middle Jurassic, the EAB recorded three transgression-regression cycles. The first transgressive-regressive cycle occurred during the Sinnemurian-Pliensbachian and was truncated by the Toarcian erosion which marks the beginning of the Toarcian transgression. This transgression culminate with subtidal deposits at the end of the Toarcian and is followed by a regression which establish continental conditions in the South of the Basin during the Middle Jurassic. Lastly, the end of the Middle Jurassic is marked by the initiation of a stronger transgression which continues during all the Callovian.
6. Throughout the Lower and Middle Jurassic, the Rehamna, the MAM and the Anti-Atlas were exhuming (Ghorbal et al., 2008; Charton, 2018).

   The Rehamna and the MAM being the closest potential source to the EAB, they are considered to be a siliciclastic provenance area candidate for the Toarcian continental and marine siliciclastics. The Anti-Atlas source potential for the Toarcian should also be tested as its exhumation rate was high during this period of time. It was seemingly the main source of the Middle Jurassic siliciclastics.
7. These results indicate that between the Lower Pliensbachian and the Toarcian, the EAB sedimentary record supports recent published low-T thermochronology that indicates exhumation of the Meseta and Anti-Atlas.

8. The vertical movements can be correlated with phases of siliciclastic input into the basin, providing evidence that the Atlantic Passive Margin was experiencing vertical tectonic movements during the syn-rift and post-rift phase. This illustrates that controls on accommodation in a passive margin can be influenced by tectonics in the hinterland and do not only depend on global eustasy.

Acknowledgments: This study formed part of the lead author’s PhD at the University of Manchester. It forms part of the North Africa Research Group (NARG) project on the Mesozoic Evolution of the Moroccan Atlantic Margin. The authors would like to express their gratitude to the sponsoring companies of NARG for their financial and scientific support and to The Office National des Hydrocarbures et des Mines (ONHYM) for their logistical and scientific support, in particular Mr Nahim, Ms Habid and Mr Aabi.

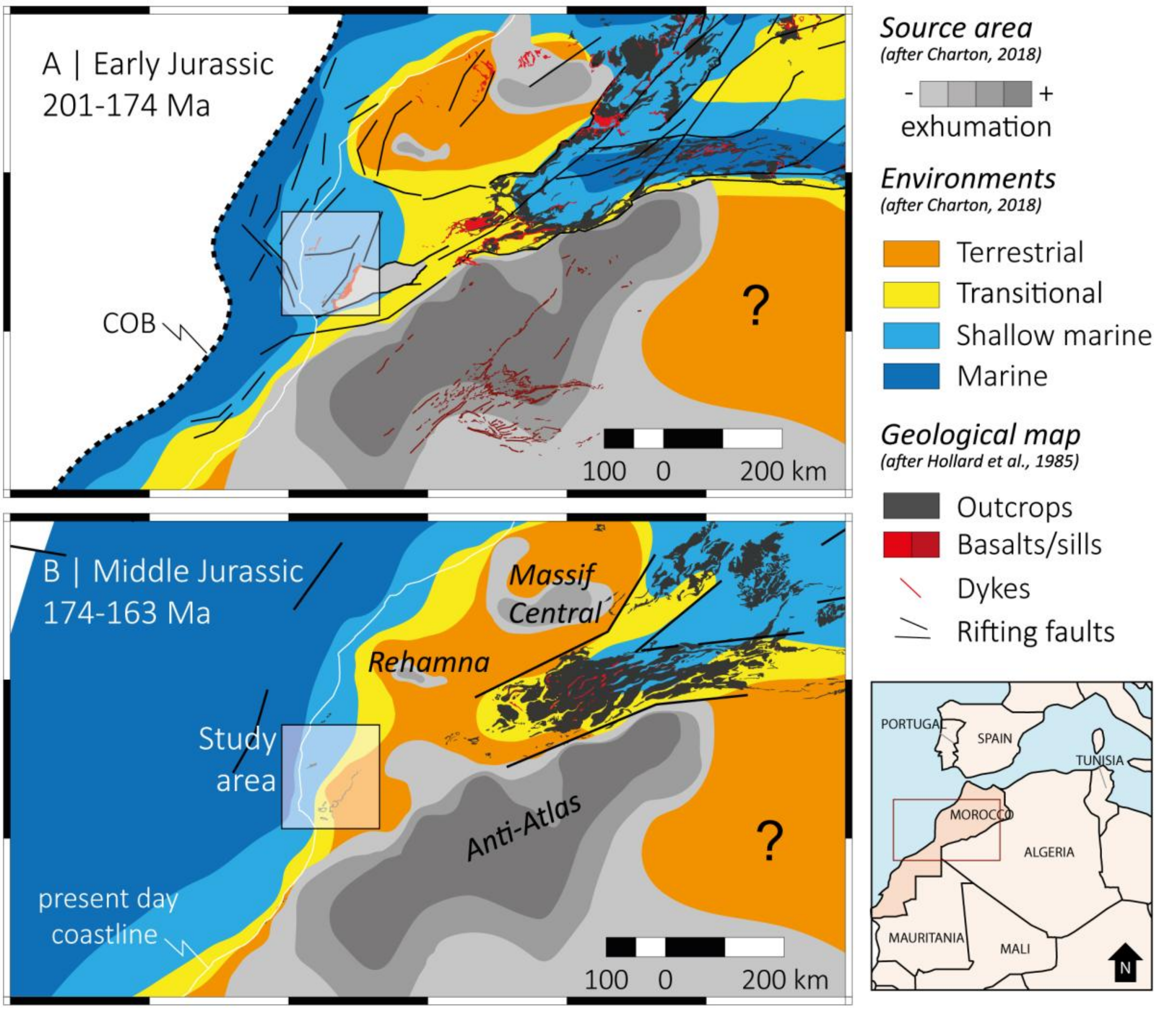

Figure 1: Paleogeographic maps of the Central Western Morocco for the Lower Jurassic (A) and Middle Jurassic (B). After Charton, 2018. Location of study area.

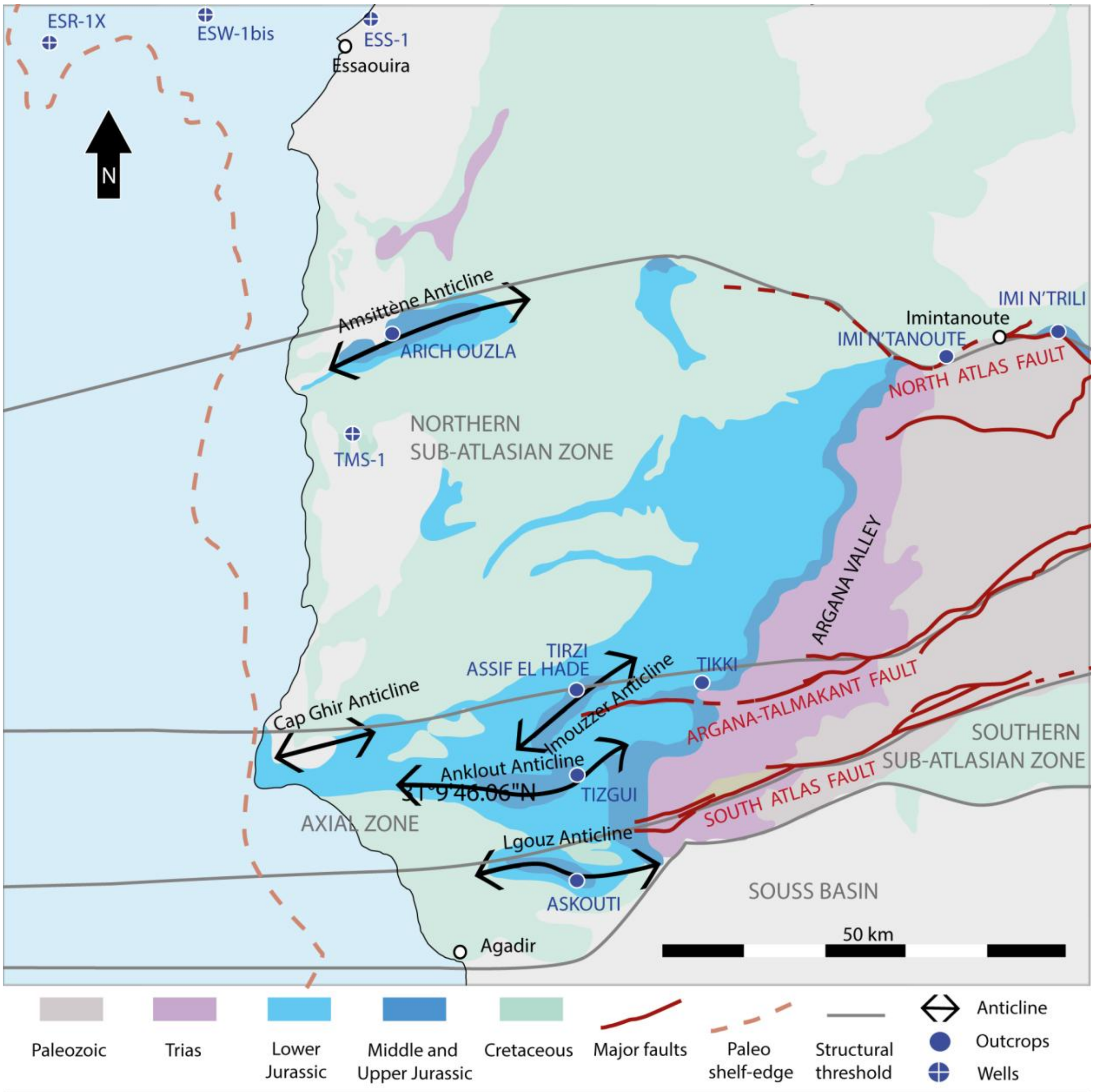

Figure 2: Geological map of the Essaouira-Agadir Basin (modified after Choubert, 1957; Zühlke et al., 2004) and location of the wells and outcrops studied. Fault location from the geological maps 1:10000 of Imi'n Tanoute, Argana and Khemis Meskala. Paleoshelf-edge from Hafid et al. (2006). The basin is divided into three zones, the Southern sub-atlasian Zone, the Axial Zone and the Northern sub-Atlasian Zone.

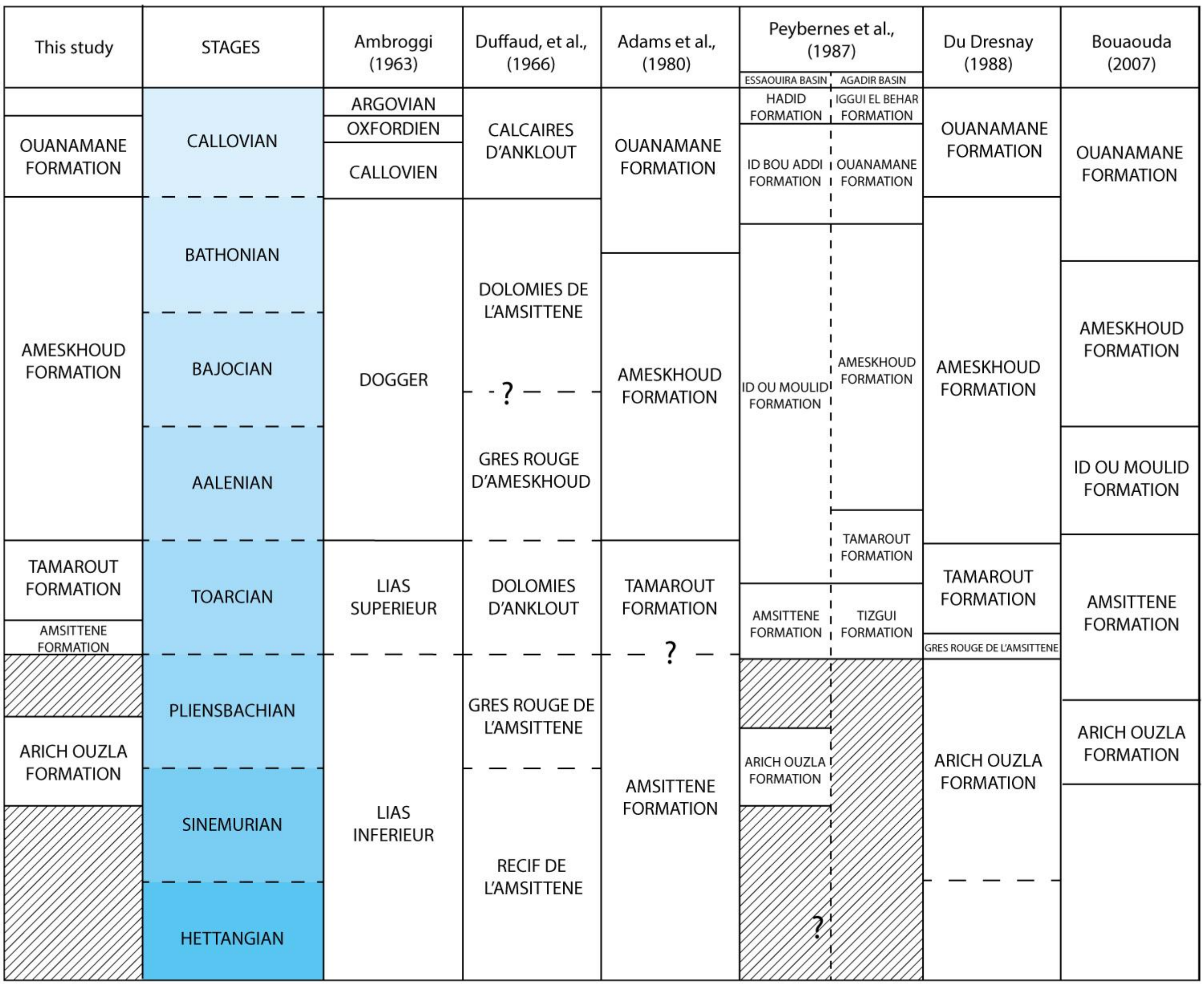

Figure 3: Lithostratigraphy of Lower and Middle Jurassic formations of the Essaouira-Agadir Basin used in the present work and compared with older stratigraphic studies (see references therein).

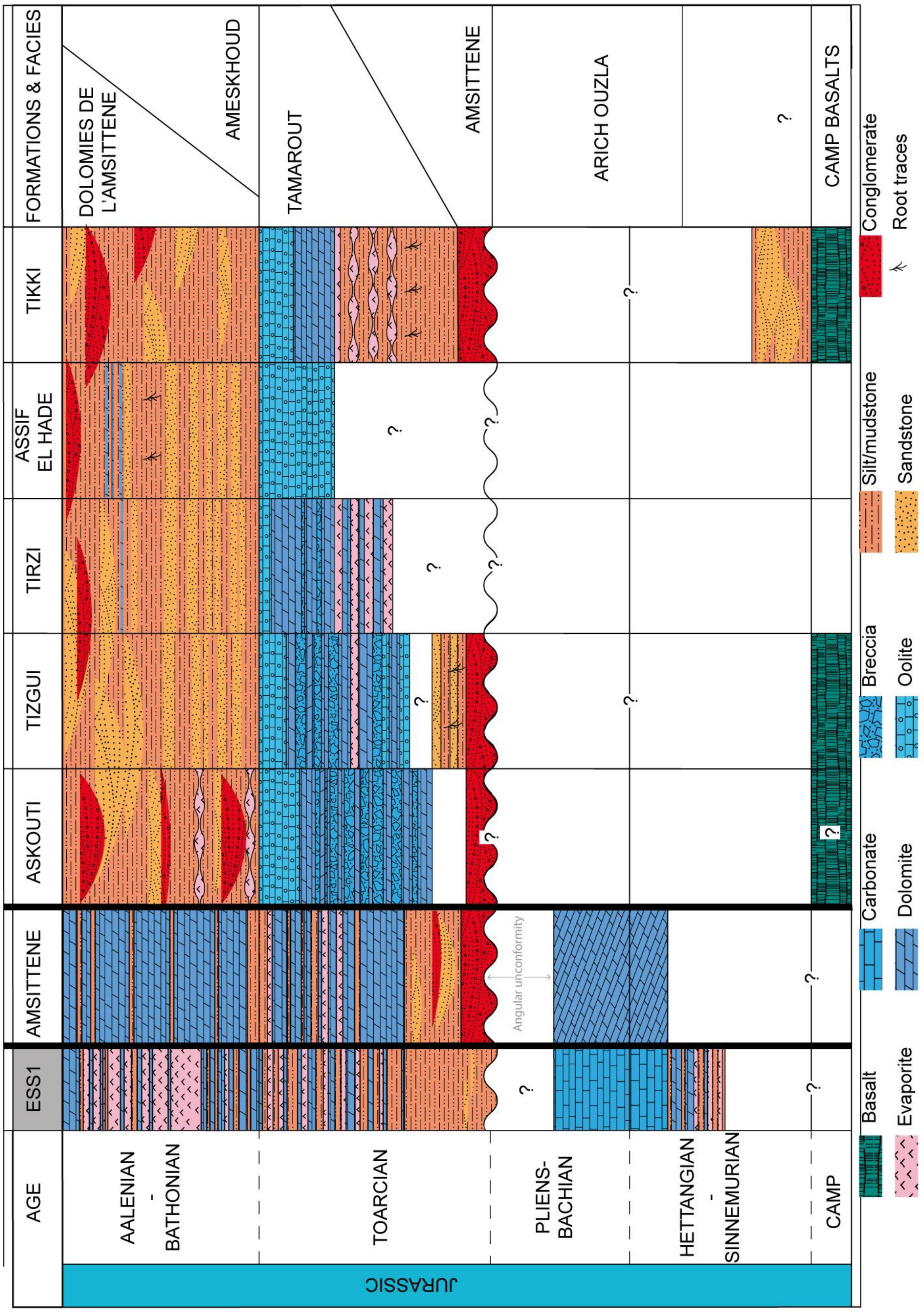

Figure 4: Chronostratigraphic chart of the Lower and Middle Jurassic in the Western High Atlas. Dating based on Ambroggi (1963), Bernoulli and Kälin (1984), Riegraf et al., (1984),

Peybernes et al., (1987), Du Dresnay; (1988), (Bouaouda, 1987, 2004, 2007). Stratigraphy of the Amsittene location from Peybernes (1987) and Du Dresnay (1988). Locations of the different sections in Fig. 3.

Lithofacies names	Diagnostic components	Matrix and porosity	Sedimentary features and bioturbation	Beds thickness and Observations	FA1	FA2
LFAO1 Dolomitic oolite	Dolomitic recristallized ooids and peloids In more dolomitised beds: phantoms of rounded grains (Ø 50-100 µm)	Micrite, euhedral and subhedral Homogenoeous euhedral crystals Intercristalline porosity 10-20%	Thick beds, sedimentary features overprinded by dolomitisation	dm-m Massive aspect Small fractures common		
LFAO2 Dolomitic coated grains PST to FST / RST	Coated grains (oncoids?) 10-70%, Shell fragments 10-30% Peloids 5-20% Foraminifers 0-2% Gastropods 0-10% Quartz grains 0-10% In more dolomitised beds: recristallised shell fragments and phantoms of rounded grains (Ø 100-400 µm)	Micrite matrix, partially dolomitised Fractures filled by blocky calcite Homogenoeous euhedral crystals Intercristalline porosity 10-20%	Horizontal bedding Massive Horizontal laminations	cm-m Massive aspect Fractures common		
LFAO3 Oncoidal RST	Oncoids 50-70% Crinoids 5-10% Shell fragments 5-10% Peloids 10-20% Quartz grains 5-10%	Micrite, sparite and euhedral dolomite cristals Differential diagenesis observable in the field between matrix (yellow) and oncoids (grey)	Horizontal bedding Massive Horizontal lineaments	cm Fractures filled with secondary calcite (2%)		
LFAO4 Crinoid FST	Crinoids 15-30% Oncoids 10% Coated grains 20-40% Shell fragments 5-10% Gastropods 0-5% Quartz grains 5-10% Belemnites and ammonites <1%	Micrite and sparite	Horizontal bedding Massive Crinoid-rich horizons	cm Vertical fractures filled with secondary calcite		
LFAO5 Bioclastic WST/PST GST/FST	Shell fragments 10-50% Coated grains 5-50% Crinoids fragments 2-10% Gastropods 0-5% Coral fragments 0-5% Quartz grains 0-5% Belemnites fragments 0-2% Ammonites <1%	Micrite, euhedral and subhedral dolomite cristals	Horizontal bedding Massive	cm-m Fractures Horizontal stylolites		
LFAO6 Yellow/pink dolomite	Recristallised shell fragments phantoms 10-15%	Euhedral to anhedral dolomite cristals	Thalassinoides bioturbation prefferentially recristallised	m Yellow and pink dolomite Heavilly fracturated Moldic porosity Horizontal stylolites		

Facies association	Lithofacies n°	Facies association description	Summarized facies association stratigraphy
FA1 Lagoonal	LFAO1, LFAO2	Thick units of dolomite (up to 10m) alternating with meter-thick beds of oolitic, peloidal, coated-grains and shell fragments grainstones.	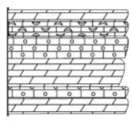
FA2 Midramp	LFAO2, LFAO3, LFAO4, LFAO5, LFAO6	Oncoidal PST, FST and RST alternating with crinoid-rich bioclastic PST to FST. Various bioclastic association of crinoids, oncoids, gastropods, bivalves, brachiopods, coral fragments, belemnites and ammonites. Locally completely recristallized, replaced by yellow and pink dolomite.	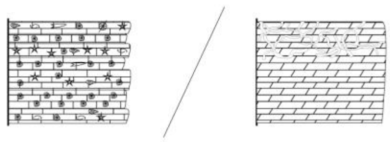

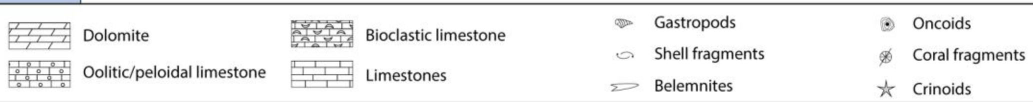

Figure 5: Lithofacies and facies associations of the Arich Ouzla Formation.

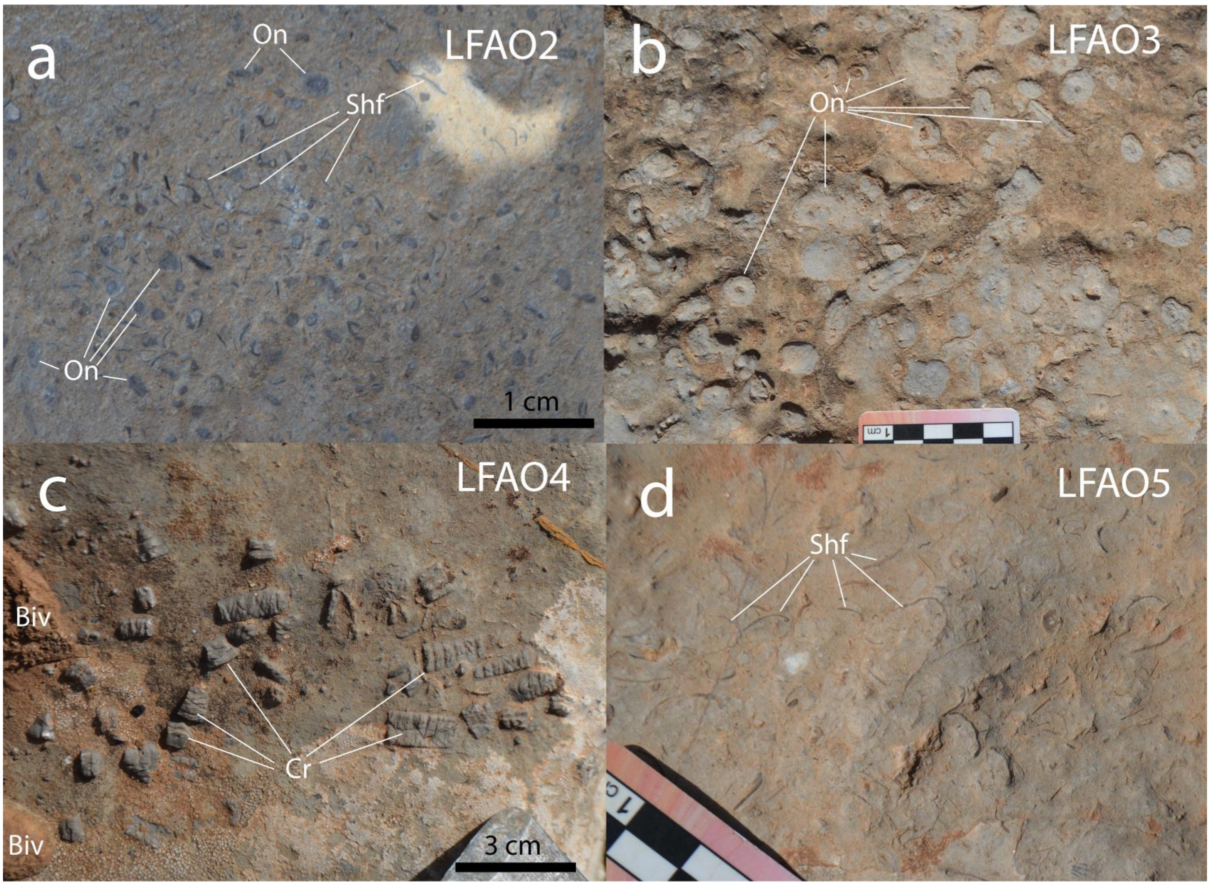

Figure 6: Lithofacies of the Arich Ouzla Formation. Facies LFAO2, oncolith (On) PST and shell fragments (Shf)(a); Facies LFAO3, oncoidal RST with shell fragments (b); Facies LFAO4, crinoids (Cr) and bivalves (Biv) FST (c); Facies LFAO5, bioclastic FST with thin shell fragments (Shf) (d).

Lithofacies name Texture	Main elements	Sedimentary features	Observations and bed thickness	FA3	FA4	FA5
LFAT1 Quartzite conglomerates	Quartzite pebbles and cobbles, well rounded, poorly sorted conglomerates, clast-supported, polymodal, medium sandstones and granules matrix Pebbles: Quartzite 99%, Metabasalt and basalt 1%	Cross-bedding and parallel laminations in conglomerate Erosion surfaces	Very continuous lateraly Red-pink outcrops appearance m-Dm			
LFAT2 Medium to coarse sandstones	Poorly sorted medium to coarse sandstones, sub-angular to sub-rounded, lenses and horizontal beds interbeded conglomerates	Crossbeds alternating between medium sandstones and conglomerates Planar cross bedding Trough cross-bedding	cm			
LFAT3 Fine sandstone	Fine sandstones, poorly sorted, subangular grains	Occasional nodular horizons and roots traces, paleosoils	Separate conglomeratic units cm-m			
LFAT4 Quartzites conglomerates	Quartzite pebbles and cobbles, subrounded to subangular, poorly sorted conglomerates, clast-supported, coarse sandstones matrix Pebbles, cobles : Quartzite 90%, green basalt 10% Pebble size un to 10 cm, average size 2 cm	Lenticular beds planar cross-bedding low angle cross-bedding massive Erosive base	Disappear laterally 30 cm -2 m thick			
LFAT5 Coarse sandstones	Poorly sorted coarse sandstones with granules, sub-rounded to subangular	Planar cross bedding Trough cross-bedding	5-30 cm			
LFAT6 Medium to coarse sandstones	Moderately sorted medium sandstones fining upward to fine sandstones	Assymetric current ripples Planar cross-bedding	5-15 cm			
LFAT7 Red clay and siltstones	Red clay and siltstones alternating in thin horizons Thicker horizons of clay with thin cm-thick horizons of red silt Horizons of clay coarsening upward to silt	Horizontal laminations Current ripples in silt lenses	Locally laterally passing to conglomerates 50 cm -5 m			
LFAT8 Very fine sandstones	Very fine sandstones or fine sandstones Thin horizons alternating with silt horizons and thicker beds thinning upward to silt Locally small carbonate cement content	Current ripples Flaser bedding	Red colour dominating, occasionaly grey-green cm-m			
LFAT9 Fine sandstones	Fine sandstones horizons alternating with thin (20 cm) silt horizons	Low angle tabular cross-laminations Climbing ripples with sinuous crests	30 - 40 cm			
LFAT10 Matrix-suppported conglomerates	Matrix-supported conglomerates, thinning upward, quartzite and silty pebbles	Tabular cross bedding Cross-laminations	50 cm - 1.5 m			

Facies association	Lithofacies n°	Facies association description	Summarized facies association stratigraphy
FA3 Alluvial fan	LFAT1, LFAT2, LFAT3	Massive and cross-bedded plurimetric quartzite conglomerates with poorly sorted, cross-bedded medium sandstones lenses, separated by continuous centimeter to meter thick fine sandstones.	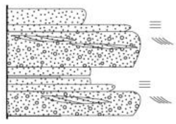
FA4 Braided river	LFAT4, LFAT5, LFAT6	Repeated fining-upward conglomerates and sandstones. Lenticular conglomerates with an erosive base and cross-beds, fining to coarse sandstones with trough and planar cross-bedding, fining to medium and fine sandstones with current ripples.	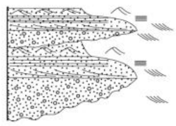
FA5 Flood plain	LFAT7, LFAT8, LFAT9, LFAT10	Facies association dominated by red clay and siltstones, interbedded with very-fine sandstones with current ripples, cross-laminations and flaser-bedding, fining upward to siltstones. Common cross-bedded fine-grained sandstones sheets and occasional matrisupported conglomerates.	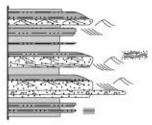

Mudstones — Silt — Sandstone — Conglomerates

Cross-bedding — Horizontal bedding — Horizontal laminations — Current ripple

Figure 7: Lithofacies and facies associations of the Amsittène Formation.

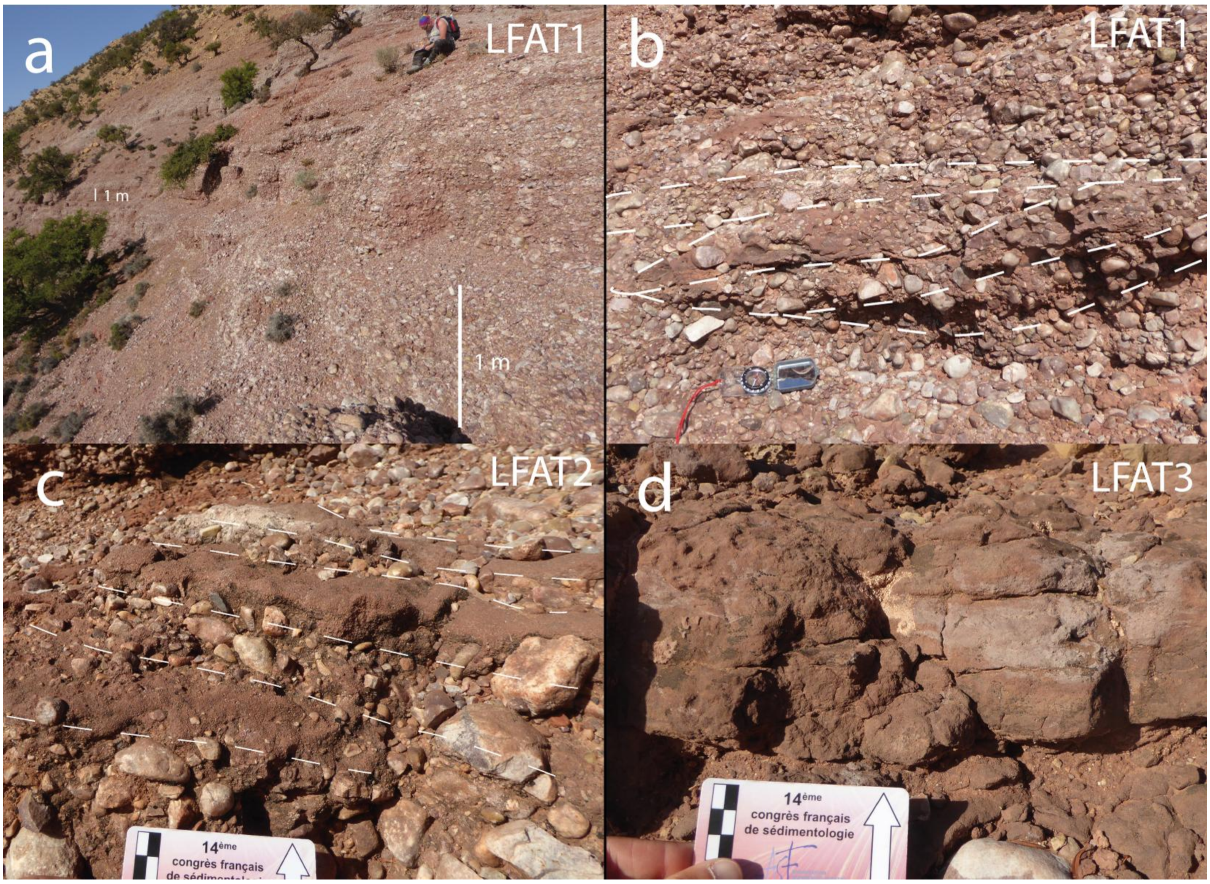

Figure 8: Lithofacies of the Amsittène Formation. Facies LFAT1, Quartzite conglomerates (a and b); Facies LFAT 2, Medium to coarse sandstones interbedded with conglomerates (c); Facies LFAT 3, Fine sandstones (d).

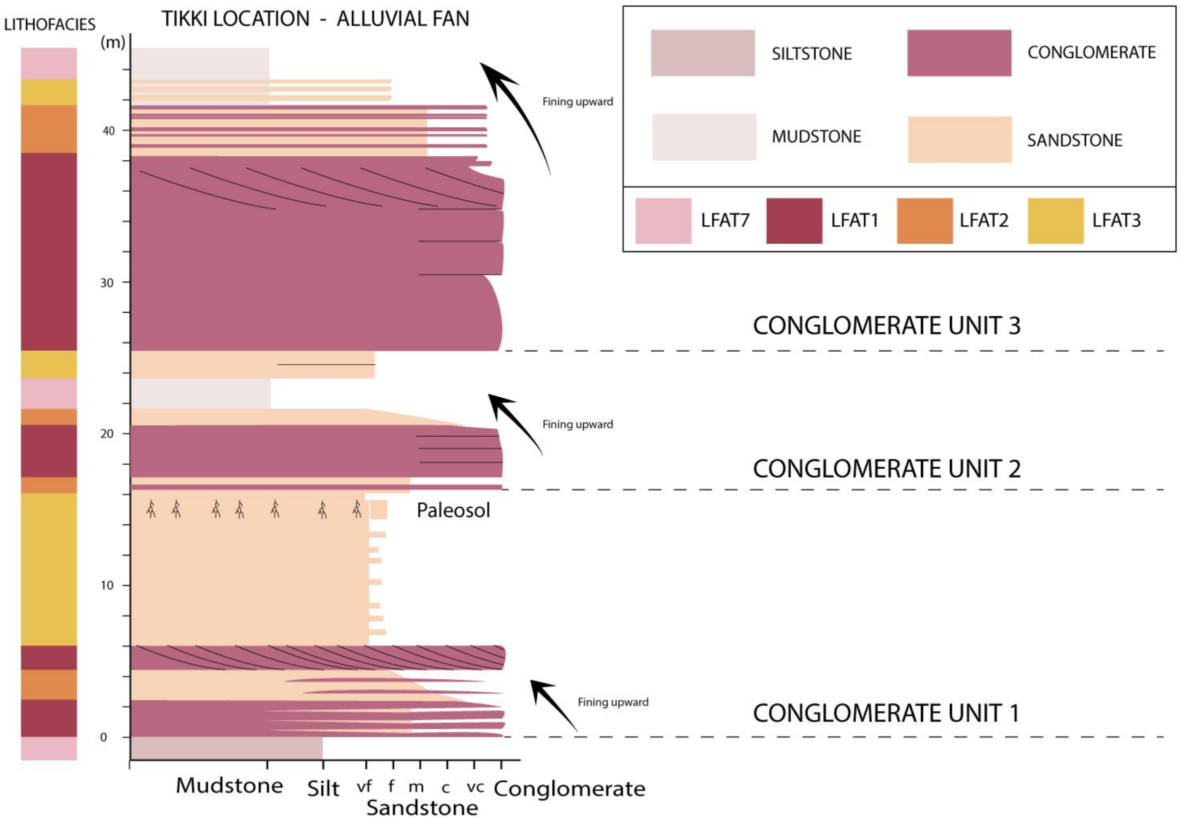

Figure 9: Simplified log of the Alluvial fans in Tikki section. The textural facies are represented in the log and the corresponding lithofacies are presented in the accompaniying lithofacies column.

Lithofacies name Texture	Main elements	Matrix	Sedimentary features and bioturbation	Beds thickness	FA6	FA7
LFTR1 Clay and marls	Red and green clays and marls	/	No bedding observed	cm-m	x	x
LFTR2 Siltstone	Red siltstones	/	Rip-up clasts Current ripples Root traces paleosoils	20 cm - 1.5 m	x	
LFTR3 Dolomitic sandstones	Dolomitic sandstones Occasional carbonate-coated grains Fine sandstones	Microspar	Planar laminations Wave ripples	20 cm - 1 m	x	
LFTR4 Sandy dolomite	Silt to fine sandstone (30-150 μm) well sorted Carbonate-coated sand grains and thin ooids (200-400 μm) 10-45%	Micrite and microspar Occasional secondary sparite cement	Planar laminations Flaser bedding, wavy bedding Tabular corss-bedding	10 cm - 80 cm	x	x
LFTR5 Evaporites nodules	Gypsum nodules horizons	/	Nodular	cm		x
LFTR6 Sandstones and siltstones	Thin horizons of very fine sandstones and siltstones	Microspar	No bedding observed	mm-cm		x

Facies association	Lithofacies n°	Facies association description	Summarized facies association stratigraphy
FA6 Coastal plain	LFTR1, LFTR2, LFTR3, LFTR4	Mixed succession dominated by mudstonas and marls alternating with sandy dolomite and dolomitic sandstones. This facies association is characterized by continental deposits presenting root traces, and a strong influx of siliciclastics alternating with sub-aqueous deposits, including oolitic grainstones with bi-directional flaser-bedding.	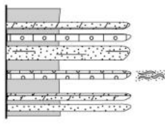
FA7 Sabkha	LFTR1, LFTR4, LFTR5, LFTR6	Red clays an siltstones interbedded with gypsum evaporites nodules. Alternation of sandstones,siltstones and micrite horizons are common, towards the top of the facies association forming cm to dm units alternating with the red clay.	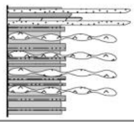

Dolomite; Sandy dolomite; Dolomitic sandstones; Silt; Oolitic limestone; Marls and mudstones; Evaporites; Flaser bedding

Figure 10: Lithofacies and facies associations of the transitional environments.

Lithofacies name	Diagnostic components	Matrix	Sedimentary features and bioturbation	Observations and beds thickness	FA8	FA9
LFTA1 Dolomite	Bivalve shell fragments 0-10% Quartz rich horizons 20%, very fine to fine sand Horizons with wood fragments up to 5%	Euhedral and subhedral dolomite crystals Micrite and microspar	Thinly bedded Horizontal laminations Heavily bioturbated horizons (thalassinoides) Horizontal laminations Faint cross bedding Cross-laminations of fine sand	Dark grey, light grey and yellow crystaline dolomite Dark beds kerogenic Vuggy horizons cm-m		
LFTA2 Bioclastic WST/PST	Brachiopods, bivalves or gastropods rich horizons, elements up to 1cm, mosttly unbroken, well sorted in a micrite matrix	Micrite Occasional secondary drusy and blocky calcite	Horizontal orientation of the grains	cm		
LFTA3 Peloidal and oolitic WST/PST	Poorly to moderately sorted pelloids and ooids (Ø 50-500 µm) 30-70% Fine quartz grains 0-40% (Ø 50-300 µm) well sorted, sub-angular to sub-rounded Bivalves and brachiopods 0-10% Rare echinoderm fragments 0-2%	Dolomitic granular and equant mozaic cement Occasional post-dolomitisation ferroan calcite cement In some sections, sparitic and micro-sparitic dolomite cement replaces the original calcite grains	Peloids and ooids wavy bedding and lenticular bedding in muddy matrix Horizontal laminations with fine sand horizons	cm-m		
LFTA4 Pelloidal GST	Well sorted pelloids 30-70% Fine quartz (Ø 50-300 µm) well sorted 0-40% sub-angular to sub-rounded	Micrite and microcristalline rhombic cement	Massive beds and herringbones cross-stratification with peloids Low angle cross stratification of fine sand and peloids Wave-formed cross-laminations with discordant internal laminae	cm-m Intercristalline porosity (0-1%)		
LFTA5 Oolitic GST	Medium to well sorted ooids, peloids and aggregates, beds with ooids quartz nuclei Beds with distorted ooids 0-20% shell fragments oriented parallel to the bedding Fine quartz , angular to subrounded 0-15% Presence of authigenic quartz 0-5%	Dolo-sparite equigranular around the grains and larger calcite blocky cement between the grains	Swalley cross-stratifications Cross-bedding 5-40 cm Cross-laminations Horizontal laminations Wave ripples	cm-m		
LFTA6 MST	MST clasts	Micrite with 0-15% clay content	Occasional horizontal bioturbation	cm		
LFTA7 Marls	Green and grey marls	/	No bedding observed	cm		
LFTA8 Stromatolites	Dark micritic horizons	Micrite and microspar alternating	Stratiform irregular laminations	Kerogenic cm		
LFTA9a Evaporites	Gypsum beds Thin mm thick horizons of grey MST and inclusions of MST granules	Micrite	Waves ripples in the MST horizons Gypsum horizons massive or thinly laminated	Lateral variations of thickness Post-sedimentary deformations cm-m		
LFTA9b Breccias	Dolomitic angular pebbles and cobbles of micrite, oolitic GST and stromatolites	Micrite, sparite, euhedran and anhedral dolomite cristals	Breccias coarsening upward, top bed of the breccia horizon usually less broken	Lateraly discontinuous beds, breccia lenses Layers above unaltered cm-m		

Facies association	Lithofacies n°	Facies association description	Summarized facies association stratigraphy
FA8 Subtidal	LFTA1, LFTA2, LFTA3, LFTA4, LFTA5, LFTA7	Thick units of dolomite (up to 10m) alternating with cm-m thick beds of oolitic and peloidal grainstones. Marls and bioclastic limestones common.	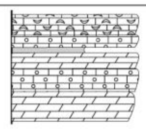
FA9a/FA9b Supratidal Intertidal	LFTA3, LFTA4, LFTA5, LFTA6, LFTA8, LFTA9a/LFTA9b	Oolitic grainstones, dolomite and breccia domination. Stromatolites followed by thick evaporites (FA8a) or dissolution breccias (FA8b) alternating with units of oolites and dolomites.	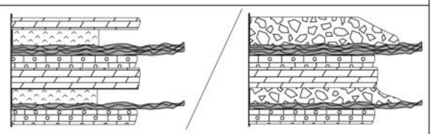

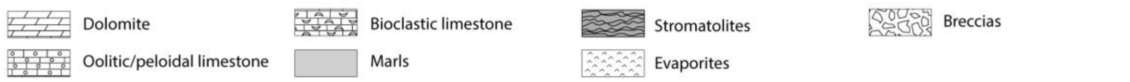

Figure 11: Lithofacies and facies associations of the Tamarout Formation.

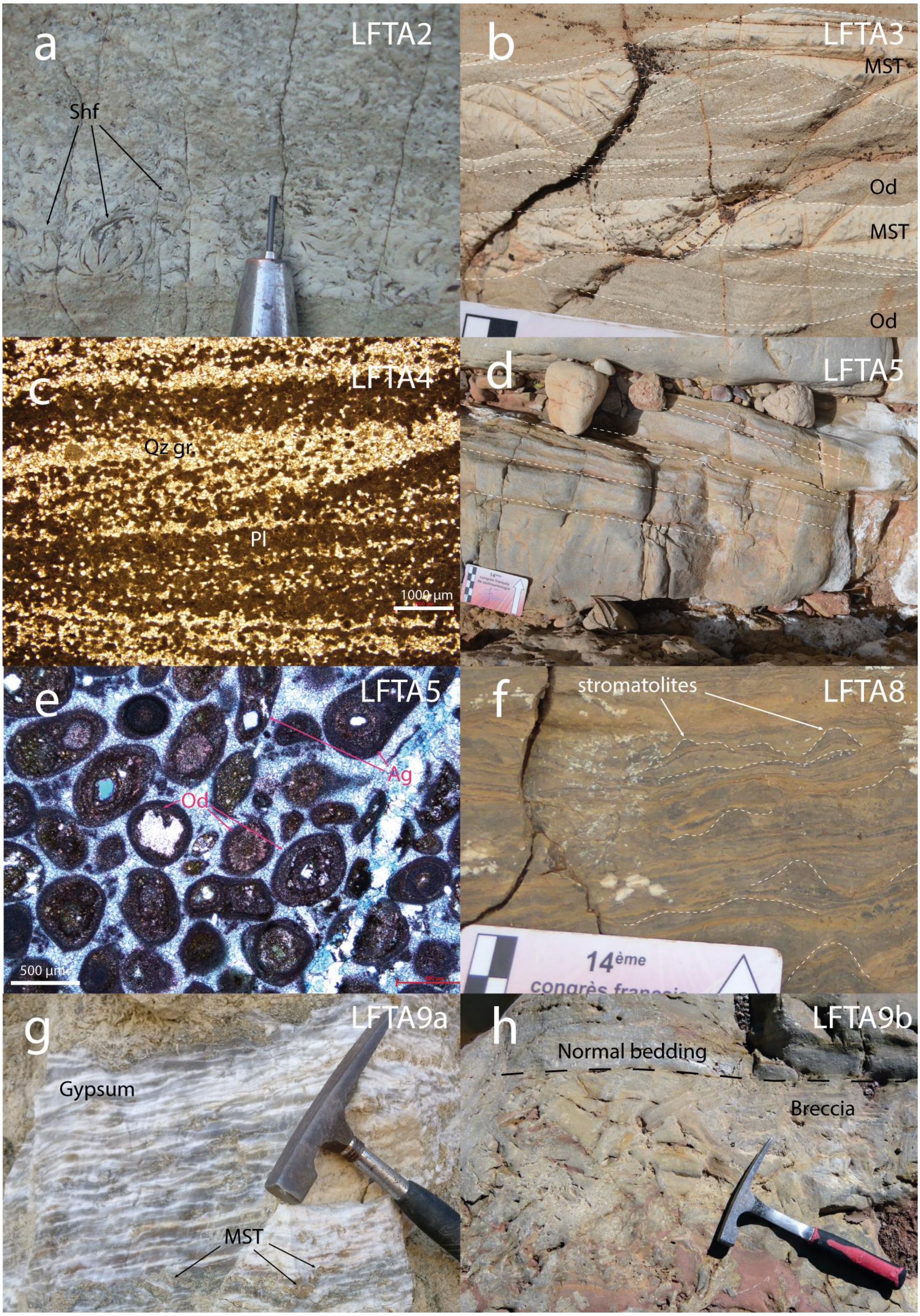
a
LFTA2
Shf
b
LFTA3
MST
Od
MST
Od
c
LFTA4
Qz gr.
Pl
1000 µm
d
LFTA5
e
LFTA5
Ag
Od
500 µm
f
LFTA8
stromatolites
14ème
congrès franç
g
LFTA9a
Gypsum
MST
h
LFTA9b
Normal bedding
Breccia

Figure 12: Lithofacies of the Tamarout Formation. Facies LFTA2, Bioclastic PST with mm-scale bivalves shell fragments (a). Facies LFTA3, wavy-bedded oolitic WST/PST (b). Facies LFTA4, wave ripples in peloidal and fine sand GST (c). Facies LFTA5, cross-beds in oolitic GST (d and e), ooids (Od) and aggregates (Ag). Facies LFTA8, Stromatolites (f). Facies LFTA9a, Evaporites (g). Facies LFTA9b, dissolution-collapse breccias with carbonate mudstone (MST) nodules (h).

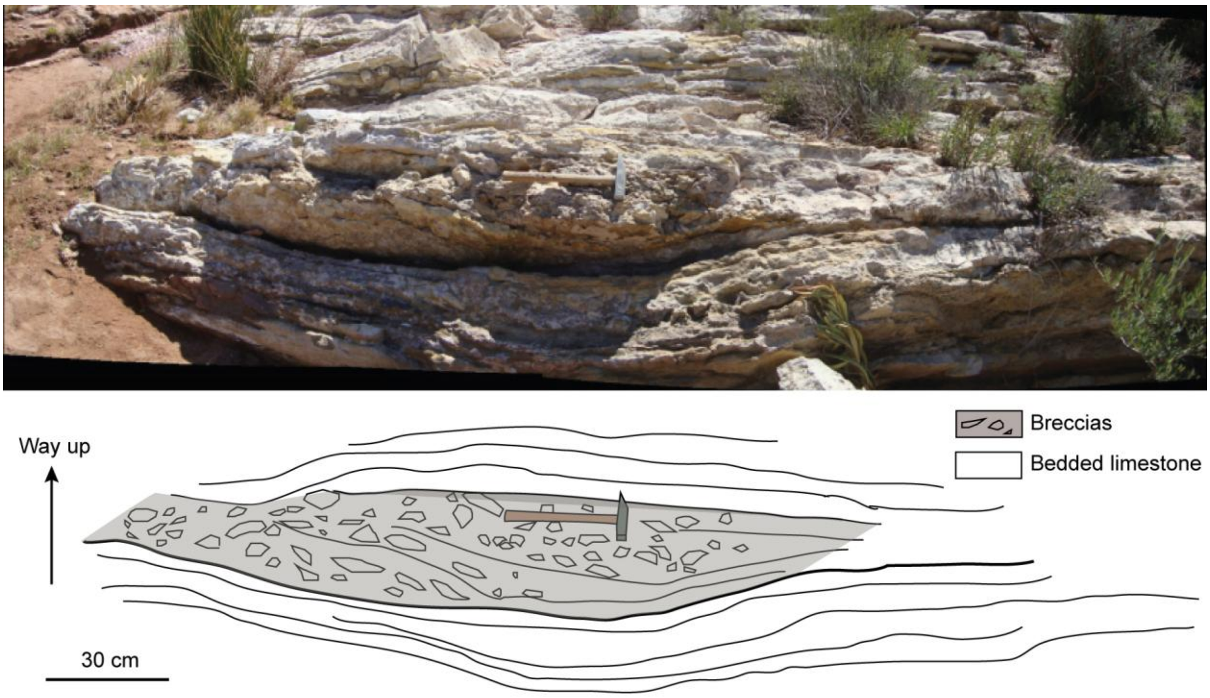

Figure 13: Example of lenticular breccia bed and associated syn-sedimentary ductile folding in the Tamarout Formation.

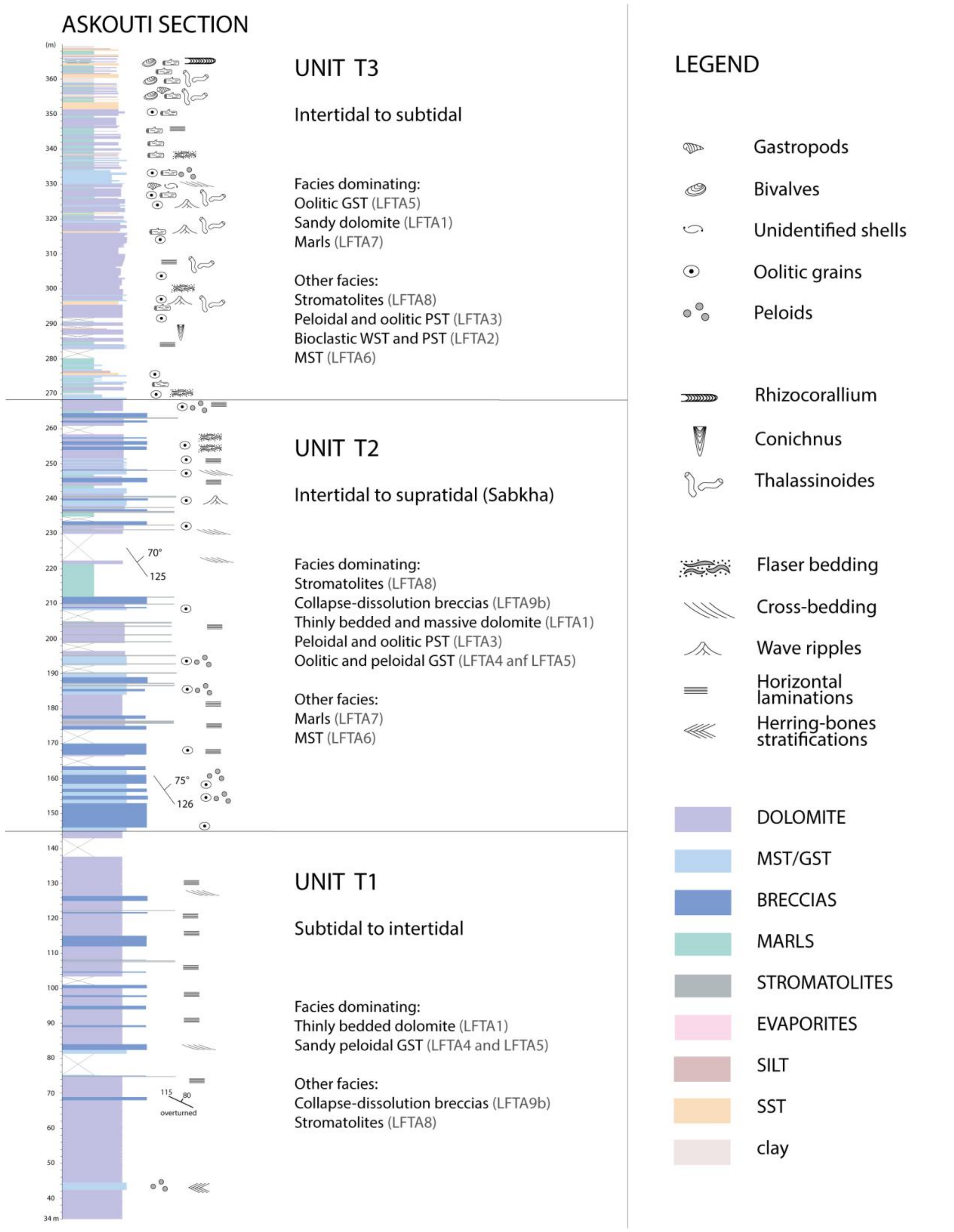

Figure 14: Askouti lithologic section and sedimentary structures, divided into the Units T1, T2 and T3, the three units of the Tamarout Formation distinguished by different dominating facies, facies organisation and stratigraphic position.

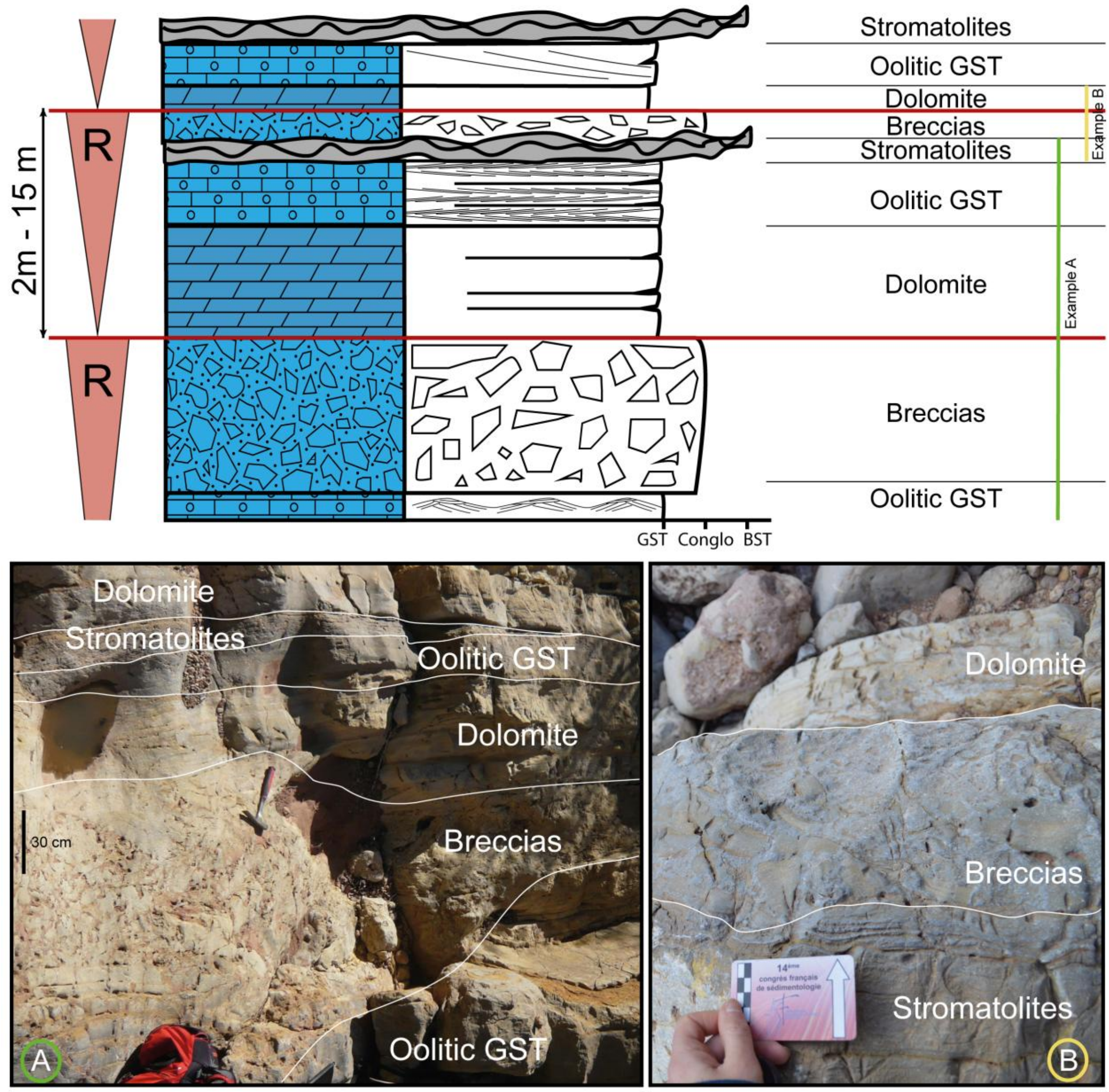

Figure 15: Examples of peritidal cycles in the Tamarout Formation. A and B examples from Askouti location.

Lithofacies name	Main elements	Sedimentary features and bioturbation	Beds thickness and observations	FA10	FA11
LFAK1	Red mudstone Occasional carbonates nodules	Massive Horizontal parallel bedding	2 cm - 5 m		
LFAK2	Siltstone, occasional very fine sand intervals	Horizontal parallel bedding Low angle cross-bedding, Wave ripples	10 cm - 10 m		
LFAK3	Very fine to very coarse sandstone, well to moderately sorted Occasional dolomitic matrix	Horizontal parallel bedding Low angle cross-bedding Occasional irregular base, continuous Wave ripples, Cross-bedding, mud drapes Ophiomorpha, Rhizocorallium, Diplocraterion	10 cm - 8 m Horizons with vugs and nodules		
LFAK4	Fine to very coarse sandstones, moderately to poorly sorted, red clay mud-clasts, quartz granules	Erosive base, lenticular, fining-upward, top bioturbated Thalassinoides Planar and trough cross-bedding current-ripples, ripple-drift cross-lamination	20 cm - 70 cm Lateral extent up to 10 m		
LFAK5	Fine to coarse sandstones, well sorted	Flat top and base, horizontal bedding, trough cross-bedding ripple laminations, mud drapes bidirectional cross-bedding Occasional root traces Thalassinoides,Arenicolites	10 cm - 50 cm		

Facies association	Lithofacies n°	Facies association description	Summarized facies association stratigraphy
FA10 Near shore	LFAK1, LFAK2, LFAK3	Continuous beds of red clay, siltstones and sandstones. Massive and horizontal parallel bedding of the clay and siltstones. Common wave ripples and low angle cross-bedding in the siltstones and sandstones. Bioturbation in the sandstones: Ophiomorpha, Rhizocorallium, Diplocraterion	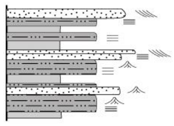
FA11 Tidal flat	LFAK1, LFAK2, LFAK4, LFAK5	Thick red clay intervals, with interbedded silt and sandstones. Sandstones and siltstones well to poorly sorted, with horizontal bedding, cross-bedding and current ripples. Some lenticular, erosive, fining-upward medium to coarse sandstones with granules or mud clasts at the base. Occasional root traces. Bioturbation in the sandstones: Thalassinoides and Arenicolites	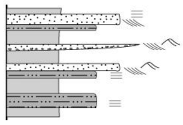

Mudstones	Silt	Sandstone	Wave ripple
Cross-bedding	Horizontal bedding	Horizontal laminations	Current ripple

Figure 16: Lithofacies and facies associations of the Ameskhoud Formation.

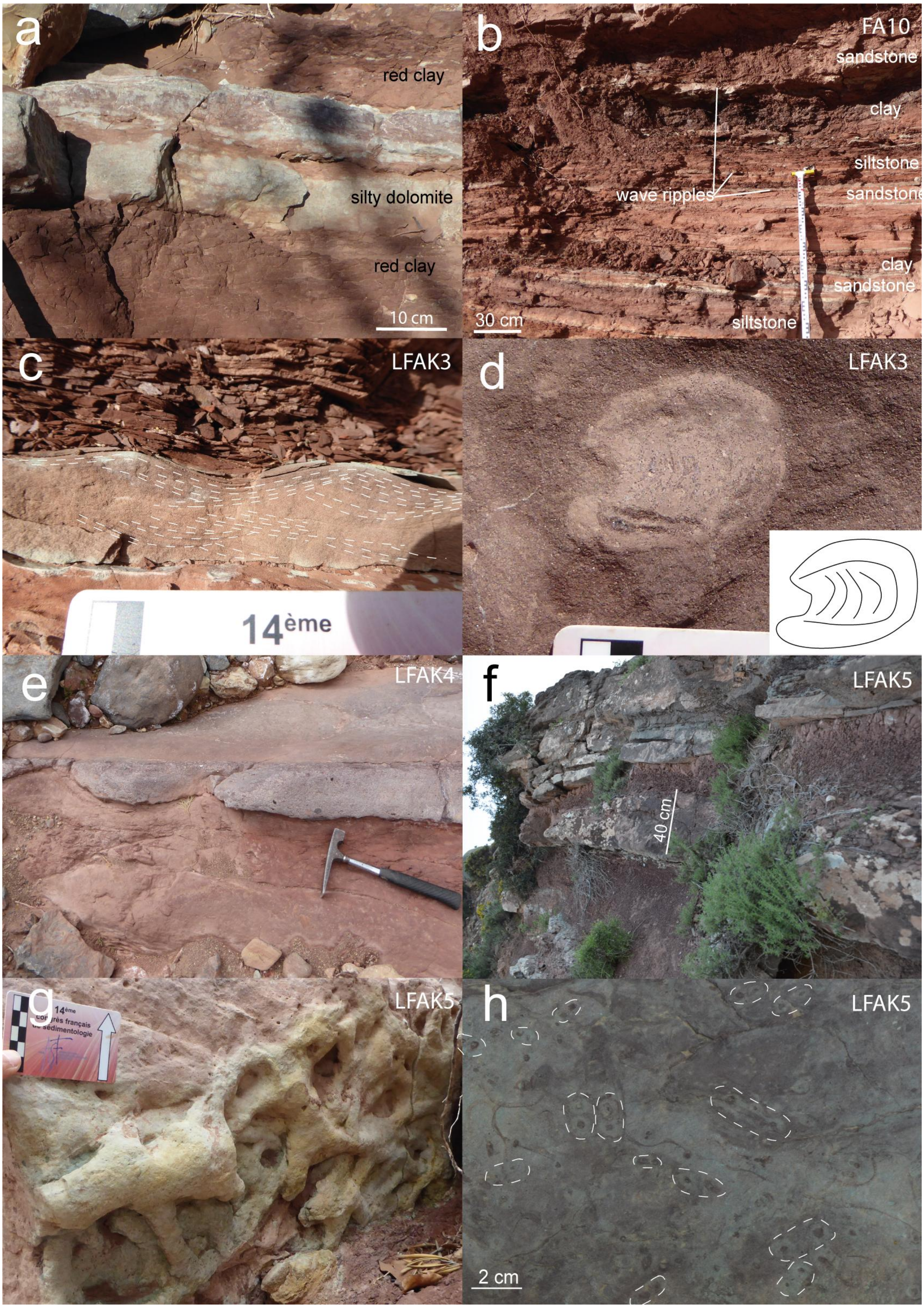

Figure 17: Ameskhoud Formation facies. Alternation of silty dolomite and red clay at the base of the formation (a). Thinly bedded red clay, siltstone and sandstones with waves

ripples, FA10 (b). Waves ripples (c). *Rhizorocallium* burrow (d). Small channelized sandstone with rip-up clasts interbeded with red clay (e). Fine sandstones and red clay alternation in the upper part of the formation (f). Roots traces (g). Arenicolites burrows (h).

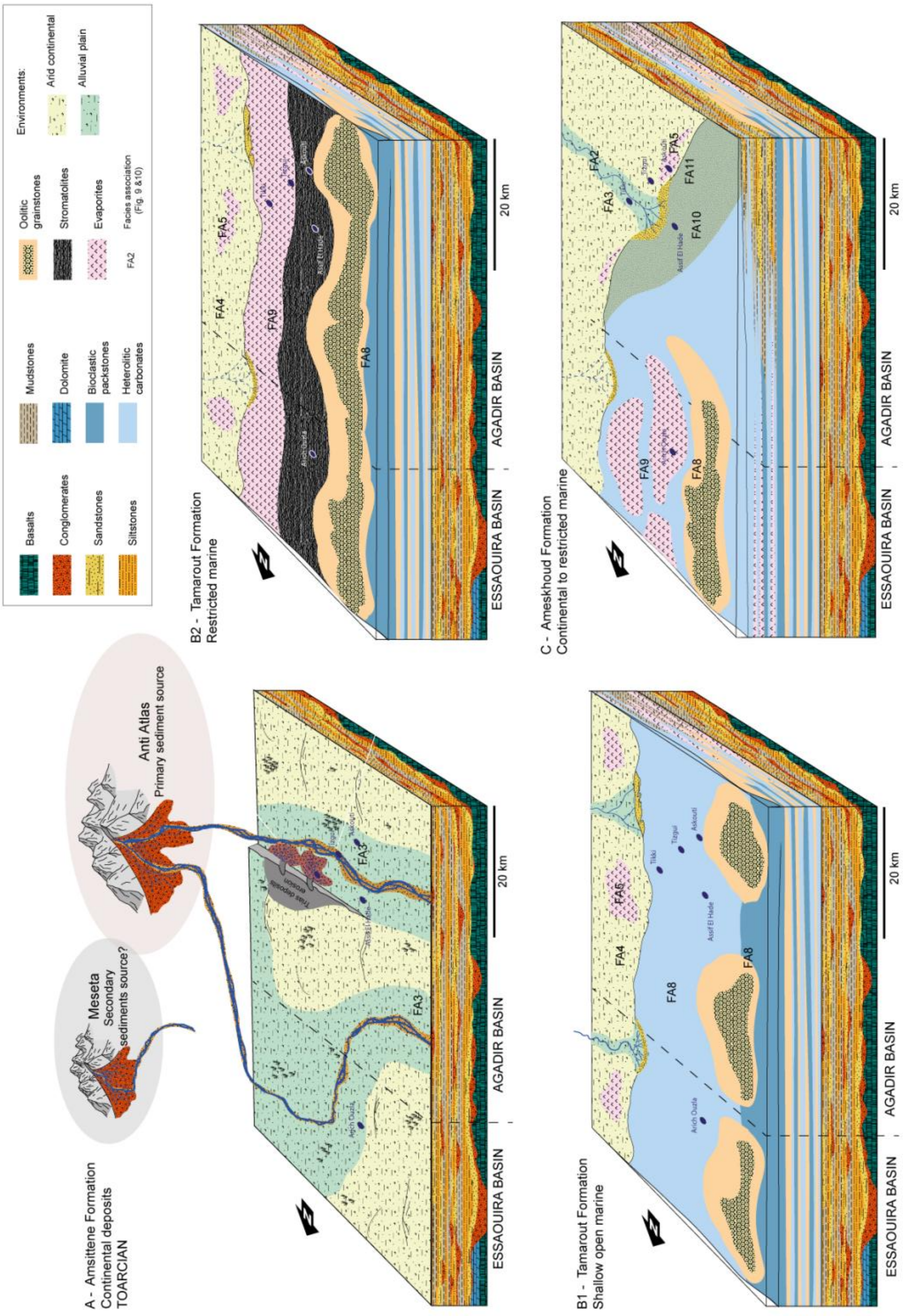

Figure 18: Depositional environments for the continental Amsittène Formation (A), the intertidal to supratidal Tamarout Formation (B1 and B2) and siliciclastic Ameskhoud Formation in the south and corresponding carbonate environoments in the north (C).

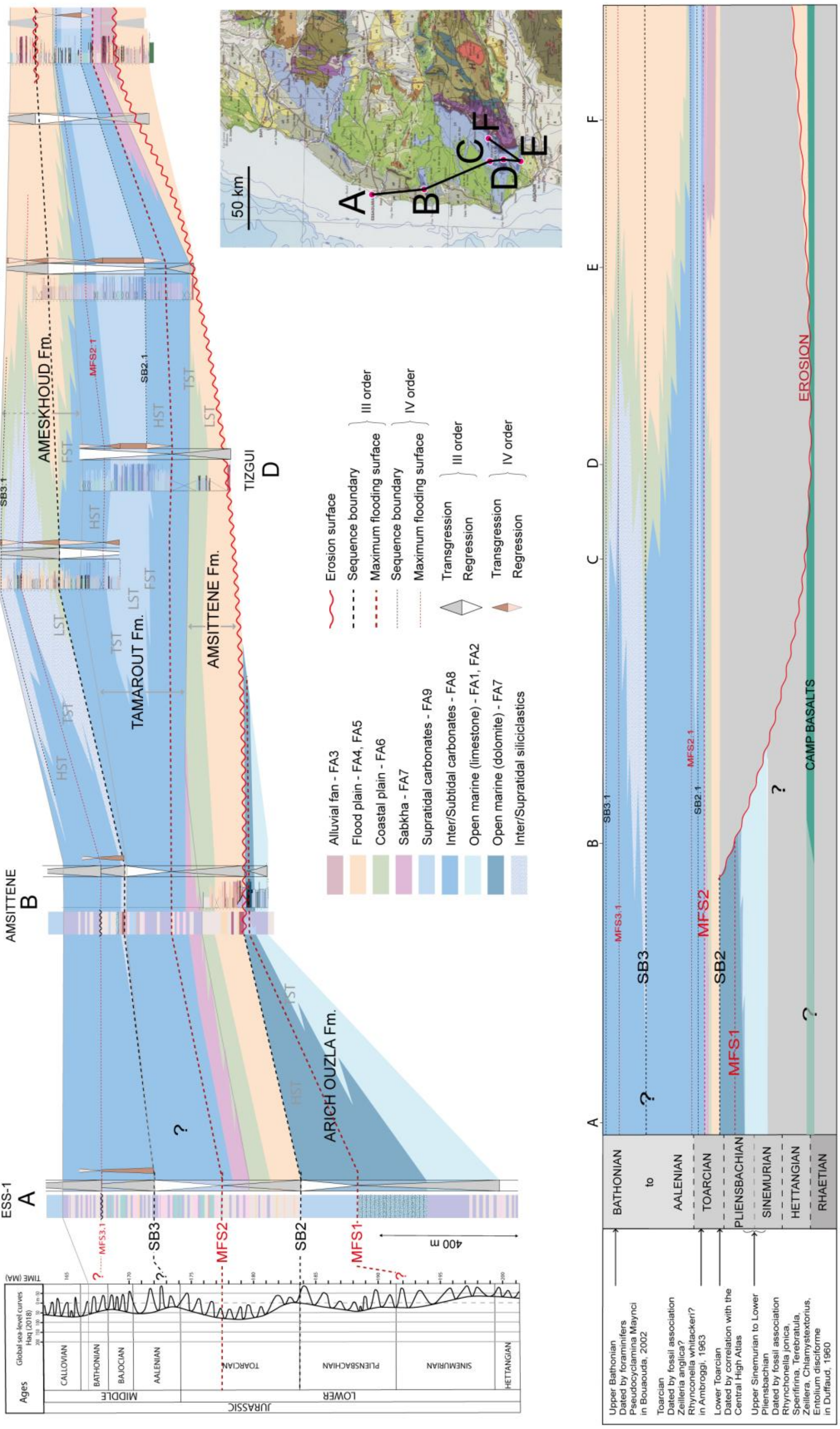

Figure 19: Lower and Middle Jurassic stratigraphic correlations between the well Essaouira-1, Amsittène, Assif El Hade, Tizgui, Askouti and Tikki, and the associated Wheeler diagram

Data are referenced to the chronostratigraphic framework based on the references therein. Correlations of the main stratigraphic surfaces to the Haq (2018) global sea level curves. Logs in annex.

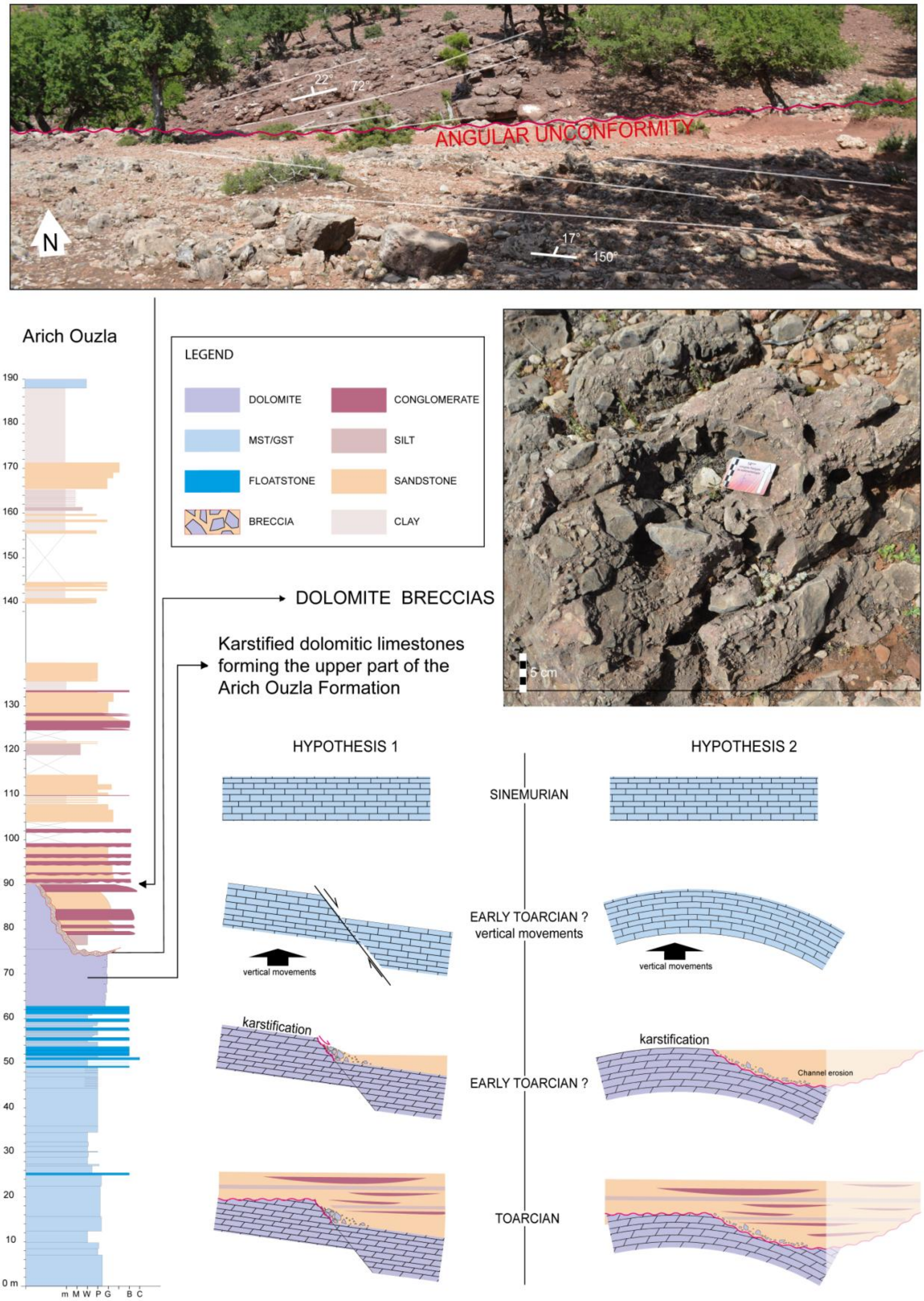

Figure 20: Schematic evolution and hypothesis on the formation of the breccias at the contact between the Arich Ouzla Formation and the Amsittène Formation.

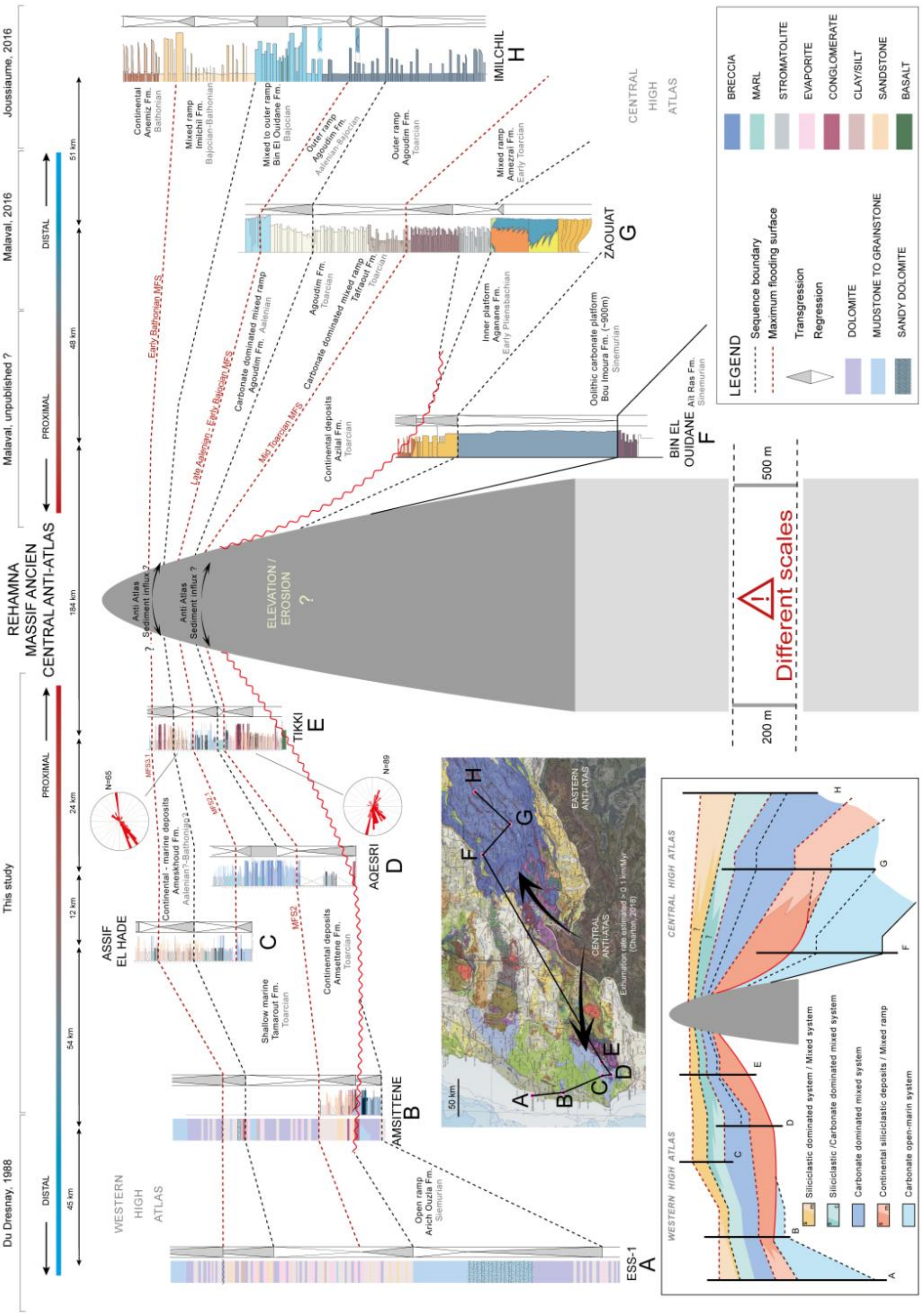

Figure 21: Western High Atlas to Central High Atlas time correlations for the Lower and Middle Jurassic (see references for the logs therein). The main different depositional packages have been highlited in different colors in the corresponding thumbnail. Proximal and distal facies are indicated. Elevation of the Anti Atlas, Rehamna and Massif Ancien produced a high between the two basins, figurated in grey.

Bibliography

Adams, A.E., 1979. Sedimentary environments and palaeogeography of the Western High Atlas, Morocco, during the Middle and Late Jurassic. Palaeogeography, Palaeoclimatology, Palaeoecology 28, 185–196.

Adams, A.E., Ager, D.V., Harding, A.G., 1980. Géologie de la région d'Imouzzer des Ida-ou-Tanane (Haut-Atlas occidental). Notes et Mémoires du Service géologique du Maroc, Rabat, 41(285), 59–80.

Aitken, J., Flint, S., 1996. Variable expressions of interfluvial sequence boundaries in the Breathitt Group (Pennsylvanian), eastern Kentucky, USA. Geological Society Special Publication 104(1), 193–206. Doi:10.1144/GSL.SP.1996.104.01.12

Al Sinawi, N., Hollis, C., Duval-Arnould, A., Schröder, S., Redfern, J., 2017. Dolomitization of Jurassic Carbonates in the Western High Atlas of Morocco: Processes and Implications for Reservoir Properties. AAPG ICE conference 2017, extended abstract.

Allen, J., 1963. The classification of cross-stratified units. With notes on their origin. Sedimentology, 2(2), 93–114. DOI :10.1111/j.1365-3091.1963.tb01204.x

Ambroggi, R., 1963. Étude géologique du versant méridional du Haut-Atlas occidental et de la plaine de Souss. Notes et Mémoires du Service géologique du Maroc, Rabat, 157, 1-321.

Arantegui, A. I. 2018. Characterisation of Mesozoic Depositional Systems along the Atlantic Passive Margin of Morocco. North Aaiun-Tarfaya Basin. PhD thesis, The University of Mannchester. 169 pp.

Ashley, G.M., Southard, J.B. and BooTHRoyD, J.C., 1982. Deposition of climbing-ripple beds: a flume simulation. Sedimentology, 29(1), pp.67-79. DOI: 10.1111/j.1365-3091.1982.tb01709.x

Baudon, C., Redfern, J., Van Den Driessche, J., 2012. Permo-Triassic structural evolution of the Argana Valley, impact of the Atlantic rifting in the High Atlas, Morocco. Journal of African Earth Sciences 65, 91–104. DOI:10.1016/j.jafrearsci.2012.02.002

Belperio, A.P., Gostin, V.A., Cann, J.H., Murray-Wallace, C.V., 1988. Sediment-organism zonation and the evolution of Holocene tidal sequences in southern Australiade Boer, P.L., Van Gelder, A., Nio, S.D. (Eds.), In: Tide-influenced sedimentary environments and facies. D. Reidel Publishing Company, Dordrecht, Holland, pp. 475–497.

Bernoulli, D., Kälin, O., 1984. Jurassic sediments, Site 547, Northwest African margin: remarks on stratigraphy, facies and diagenesis, and comparisons with some tethyan equivalents. Initial Report Deep Sea Drilling Project, Washington, 79 (13), 437-448. DOI:10.2973/dsdp.proc.79.1984

Best, J., Ashworth, P., Bristow, C., Roden, J., 2003. Three-Dimensional Sedimentary Architecture of a Large, Mid-Channel Sand Braid Bar, Jamuna River, Bangladesh. Journal of Sedimentary Research 73(4), 516–530. DOI:10.1306/010603730516

Beukes, N., Lowe, D., 1989. Environmental control on diverse stromatolite morphologies in the 3000 Myr Pongola Supergroup, South Africa. Sedimentology 36(3), 383–397. DOI:10.1111/j.1365-3091.1989.tb00615.x

Blackburn, T.J., Olsen, P.E., Bowring, S.A., McLean, N.M., Kent, D.V., Puffer, J., McHone, G., Rasbury, E.T., Et-Touhami, M., 2013. Zircon U-Pb geochronology links the end-Triassic extinction with the Central Atlantic Magmatic Province. Science 340 (6135), 941–945. https://doi.org/10.1126/science.1234204.

Blair, T., 1999. Cause of dominance by sheetflood vs. debris-flow processes on two adjoining alluvial fans, Death Valley, California. Sedimentology 46(6), 1015–1028. DOI:10.1046/j.1365-3091.1999.00261.x

Blair, T. C., Mc Pherson J. G., 1994. Alluvial fans and their natural distinction from rivers based on morphology, hydraulic processes, sedimentary processes, and facies assemblages. Journal of Sedimentary Research 64 (3a), 450-489. DOI:10.1306/D4267DDE-2B26-11D7-8648000102C1865D

Blair, T.C. and McPherson, J.G., 2009. Processes and forms of alluvial fans. In Geomorphology of desert environments. Springer, Dordrecht. 413-467. DOI: 10.1007/978-1-4020-5719-9_14

Bluck, B., 1967. Deposition of some Upper Old Red Sandstone conglomerates in the Clyde area: A study in the significance of bedding. Scottish Journal of Geology 3(2), 139–167. DOI:10.1144/sjg03020139

Boersma, J., Terwindt, J., 1981. Neap-spring tide sequences of intertidal shoal deposits in a mesotidal estuary. Sedimentology, 28(2), 151–170. DOI:10.1111/j.1365-3091.1981.tb01674.x

Bouaouda, M. S., 1987. Biostratigraphie du Jurassique inférieur et moyen des bassins côtiers d’Essaouira et d’Agadir (Marge atlantique du Maroc). Thèse de Doctorat de l’Université de Toulouse. Bouaouda, M., 2002. Micropaléontologie de la plate-forme du Bathonien-Oxfordien des régions d'Imi-N'Tanout et du Jbilet occidental (Maroc). Essai de biozonation. *Revue de paléobiologie*, *21*(1), 223-239.

Bouaouda, M.S., 2002. Micropal´eontologie de la plate-forme du Bathonien-Oxfordien des r´egions d’Imi-N’Tanout et du Jbilet Occidental (Maroc). Essai de biozonation. Rev. Paleobiol. 21 (1), 223–239.

Bouaouda, M.S., 2004. Le bassin atlantique marocain d’El Jadida-Agadir : stratigraphie, paléogéographie, géodynamique et microbiostratigraphie de la série Lias Kimméidgien. Unpublished thesis. Univ. Mohamed V, Rabat. 208pp.

Bouaouda, M. S., 2007. Lithostratigraphie, Biostratigraphie et Micropaléontologie des formations du Lias au Kimméridgien du bassin atlantique marocain d’El Jadida-Agadir, travaux de l’Institut Scientifique, Rabat, série géologie et géographie physique 22.

Bouatmani, R., Medina, F., Aït Salem, A., Hoepffner C., 2003. Thin-skin tectonics in the Essaouira basin (western High Atlas, Morocco): evidence from seismic interpretation and modelling. Journal of African Earth Sciences 37, 25-34. DOI:10.1016/S0899-5362(03)00084-8

Bridge, J. S., 1993. The interaction between channel geometry, water flow, sediment transport and deposition in braided rivers. Geological Society Special Publication., 75(1), 13–71. DOI:10.1144/GSL.SP.1993.075.01.02

Bridge, J.S., 2003. Rivers and Floodplains. Blackwell Scientific, Oxford, 504 pp. DOI:10.1002/jqs.856

Burke, K. and Gunnell, Y.,2008. The African erosion surface: a continental-scale synthesis of geomorphology, tectonics, and environmental change over the past 180 million years. Geological Society of America Memoir 201. DOI:10.1130/2008.1201

Burns, C.E., Mountney, N.P., Hodgson, D.M. and Colombera, L., 2017. Anatomy and dimensions of fluvial crevasse-splay deposits: Examples from the Cretaceous Castlegate Sandstone and Neslen Formation, Utah, USA. Sedimentary Geology, 351, pp.21-35. DOI: 10.1016/j.sedgeo.2017.02.003

Catuneanu, O., Abreu, V., Bhattacharya, J. P., Blum, M. D., Dalrymple, R. W., Eriksson, P. G., Fielding, C.R.; Fisher, W.L., Galloway, W.E., Gibling, M.R., Giles, K.A., Holbrook, J.M., Jordan, R., Kendall, C.G.St.C, Macurda, B., Martinsen, O.J., Miall, A.D., Neal, J.E., Nummedal, D., Pomar, L. 2009. Towards the standardization of sequence stratigraphy. Earth-Science Reviews 92(1-2), 1–33. DOI:10.1016/j.earscirev.2008.10.003

Catuneanu, O., Galloway, W.E., Kendall, C.G.St.C, Miall, A.D., Posamentier, H.W., Strasser, A., Tucker M.E., 2011.Sequence stratigraphy: methodology and nomenclature. Newsletters on Stratigraphy 44 (3), 173-245. DOI:10.1127/0078-0421/2011/0011

Charton, R., 2018. Phanerozoic Vertical Movements in Morocco. PhD Thesis, Delft University. DOI:10.4233/uuid:fda35870-18d9-4ca3-9443-199a1dcb0250.

Charton, R., Bertotti, G., Arantegui, A., Bulot, L., 2018. The Sidi Ifni transect across the rifted margin of Morocco (Central Atlantic): Vertical movements constrained by low-temperature thermochronology. Journal of African Earth Sciences 141, 22–32. DOI:10.1016/j.jafrearsci.2018.01.006

Charton, R., Kluge, C., Fern´ andez-Blanco, D., Duval-Arnould, A., Bryers, O., Redfern, J., Bertotti, G., 2021. Syn-depositional Mesozoic siliciclastic pathways on the Moroccan Atlantic margin linked to evaporite mobilization. Mar. Petrol. Geol. In press.

Davies, J., Marzoli, A., Bertrand, H., Youbi, N., Ernesto, M., Schaltegger, U., 2017. End-Triassic mass extinction started by intrusive CAMP activity. Nature Communications 8. DOI:10.1038/ncomms15596

Davies, P., Bubela, B., Ferguson, J., 1978. The formation of ooids. Sedimentology 25(5), 703–730. DOI:10.1111/j.1365-3091.1978.tb00326.x

Domènech, M., Teixell, A., Babault, J., Arboleya, M.-L., 2015. The inverted Triassic rift of the Marrakech High Atlas: A reappraisal of basin geometries and faulting histories. Tectonophysics 663, 177–191. https://doi.org/10.1016/j.tecto.2015.03.017.

Droser, M.L., Bottjer, D. J., 1989. Ichnofabric of sandstones deposited in high-energy nearshore environments: measurement and utilization. Palaios, 4(6). DOI:10.2307/3514750

Du Dresnay, R., 1988. Répartition des dépôts carbonatés du Lias inférieur et moyen le long de la côte Atlantique du Maroc : conséquences sur la paléogéographie de l'Atlantique naissant. Journal of African Earth Sciences 7(2), 385-396. DOI:10.1016/0899-5362(88)90083-8

Duffaud, F., 1960. Contribution à l'étude stratigraphique du bassin secondaire du Haut-Atlas occidental (Sud-Ouest marocain). Bulletin de la Société géologique de France, Paris, 2(7), 728–743. DOI: 10.2113/gssgfbull.S7-II.6.728

Dunham, R.J., 1962. Classification of carbonate rocks according to depositional textures.

Duval-Arnould, A., 2019. Controls on stratigraphic development of shelf margin carbonates: Jurassic Atlantic margin – Essaouira-Agadir Basin, Western Morocco. P.hD Thesis, The University of Manchester, 307 pp.

Embry, A.F. and Klovan, J.E., 1971. A late Devonian reef tract on northeastern Banks Island, NWT. Bulletin of Canadian petroleum geology, 19(4), pp.730-781. DOI: 10.35767/gscpgbull.19.4.705

Farrell, K.M., Harris, W.B., Mallinson, D.J., Culver, S.J., Riggs, S.R., Pierson, J., Self-Trail, J.M. and Lautier, J.C., 2012. Standardizing texture and facies codes for a process-based classification of clastic sediment and rock. Journal of Sedimentary Research, 82(6), 364-378. DOI: 10.2110/jsr.2012.30

Favre, P., Stampfli, G., 1992. From rifting to passive margin: the examples of the Red Sea, Central Atlantic and Alpine Tethys. Tectonophysics 215(1-2), 69–97. DOI:10.1016/0040-1951(92)90075-H

Fiechtner, L., Friedrichsen, H., Hammerschmidt, K., 1992. Geochemistry and geochronology of Early Mesozoic tholeiites from Central Morocco. Geologische Rundschau 81(1), 45–62. DOI:10.1007/BF01764538

Flügel, E., 2010. Microfacies of carbonate rocks: analysis, interpretation and applications. Springer- Verlag Berlin Heidelberg. 976 pp. DOI:10.1017/S0016756806221940

Folk, R. L., 1980. Petrology of Sedimentary Rocks. Austin, Texas, Hemphill Publishing Company, 182 pp.

Frazier, D.E., 1974. Depositional episodes: their relationship to the Quaternary stratigraphic framework in the northwestern portion of the Gulf Basin. University of Texas at Austin, Bureau of Economic Geology Geological Circular 71-1, 28 pp.

Friedman, G. 1997. Dissolution-collapse breccias and paleokarst resulting from dissolution of evaporite rocks, especially sulfates. Carbonates and Evaporites, 12(1), 53–63. DOI:10.1007/BF03175802

Frizon de Lamotte, D., Leturmy, P., Missenard, Y., Khomsi, S., Ruiz, G., Saddiqi, O., Guillocheau, F., Michard, A. 2009. Mesozoic and Cenozoic vertical movements in the Atlas system (Algeria, Morocco, Tunisia): An overview. Tectonophysics 475(1), 9–28. DOI:10.1016/j.tecto.2008.10.024

Frizon de Lamotte, D., Saint Bezar, B., Bracène, R., Mercier, E., 2000. The two main steps of the Atlas building and geodynamics of the western Mediterranean. Tectonics 19(4), 740-761. DOI:10.1029/2000TC900003

Gerard, J. R. F., Bromley, R. G., 2008. Ichnofabrics in Clastic Sediments: Applications to sedimentological core studies. 97 pp.

Ghorbal, B., 2009. Mesozoic to Quaternary thermotectonic evolution of Morocco (NW Africa): Vrije Universiteit Amsterdam, Ph.D. Thesis, 226 pp.

Ghorbal, B., Bertotti, G., Foeken, J., Andriessen, P., 2008. Unexpected Jurassic to Neogene vertical movements in 'stable' parts of NW Africa revealed by low temperature geochronology. Terra Nova 20, 355-363. DOI:10.1111/j.1365-3121.2008.00828.x

Goldring, R., Bridges, P., 1973. Sublittoral Sheet Sandstones. Journal of Sedimentary Research 43 (3). 736-747. DOI:10.1306/74D72856-2B21-11D7-8648000102C1865D

Gouiza, M., Charton, R., Bertotti, G., Andriessen, P., Storms, J.E.A., 2017. Post-Variscan evolution of the Anti-Atlas belt of Morocco constrained from lowtemperature geochronology: International Journal of Earth Sciences 106, 593–616. DOI:10.1007/s00531-016-1325-0

Guiraud, R., Bosworth, W., Thierry, J., Delplanque, A., 2005. Phanerozoic geological evolution of Northern and Central Africa: An overview. Journal of African Earth Sciences 43(1-3). DOI:10.1016/j.jafrearsci.2005.07.017

Hafid, M., 2000. Triassic–early Liassic extensional systems and their Tertiary inversion, Essaouira Basin (Morocco). Marine and Petroleum Geology 17(3), 409–429. DOI:10.1016/S0264-8172(98)00081-6

Hafid, M., Salem, A.A. and Bally, A.W., 2000. The western termination of the Jebilet–high Atlas system (offshore Essaouira Basin, Morocco). Marine and Petroleum Geology, 17(3), 431-443.

Hafid, M., Zizi, M., Bally, A., Ait Salem, A., 2006. Structural styles of the western onshore and offshore termination of the High Atlas, Morocco. Comptes Rendus 338(1-2), 50–64. DOI:10.1016/j.crte.2005.10.007

Hallam, A., 1981. A revised sea-level curve for the early Jurassic. Journal of the Geological Society, 138(6), 735–743. DOI:10.1144/gsjgs.138.6.0735

Halley, R.B., Harris, P.M. and Hine, A.C., 1983. Bank margin environment: Chapter 9 in Carbonate depositional environments. AAPG Memoir, 33, 463-483.

Handford, C.R., 1982. Sedimentology and evaporite genesis in a Holocene continental-sabkha playa basin—Bristol Dry Lake, California. Sedimentology *29*(2), 239-253. DOI:10.1111/j.1365-3091.1982.tb01721.x

Haq, B. U., 2018. Jurassic sea-level variations: a reappraisal. GSA today 28 (1). 4-10. DOI:10.1130/GSATG359A.1

Harvey, A., Mather, A., Stokes, M., 2005. Alluvial fans: geomorphology, sedimentology, dynamics - introduction. A review of alluvial-fan research. Geological Society Special Publication 251(1), 1–7. DOI:10.1144/GSL.SP.2005.251.01.01

Helland-Hansen, W., Gjelberg, J., 1994. Conceptual basis and variability in sequence stratigraphy: a different perspective. Sedimentary Geology 92(1-2), 31–52. DOI:10.1016/0037-0738(94)90053-1

Heward, A.P., 1978. Alluvial fan sequence and megasequence models: with examples from Westphalian D-Stephanian B coalfields, Northern Spain. In: A.D. Miall (Editor), Fluvial Sedimentology. Canadian Society of Petroleum Geology, Calgary, Alberta, 669-702. DOI:10.1002/esp.3760050213

Hoffman, P., 1976. Stromatolite Morphogenesis in Shark Bay, Western Australia. Elsevier, Developments in sedimentology 20, 261–271. DOI:10.1016/S0070-4571(08)71139-7

Hofmann, A., Tourani, A., Gaupp, R., 2000. Cyclicity of Triassic to Lower Jurassic continental red beds of the Argana Valley, Morocco: implications for palaeoclimate and basin evolution. Palaeogeography, Palaeoclimatology, Palaeoecology 161(1-2), 229–266. DOI:10.1016/S0031-0182(00)00125-5

Howard, J. D., Reineck H., 1981, Depositional facies of high-energy beach to offshore sequence: Comparison with low-energy sequence. American Association of Petroleum Geologists Bulletin, 65, 807-830. DOI:10.1306/2F919B0C-16CE-11D7-8645000102C1865D

Hunt, D., Tucker, M., 1992. Stranded parasequences and the forced regressive wedge systems tract: deposition during base-level fall. Sedimentary Geology 81(1-2), 1–9. DOI:10.1016/0037-0738(92)90052-S

Hunt, D., Tucker, M. E., 1995. Stranded parasequences and the forced regressive wedge systems tract: deposition during base-level fall - reply. Sedimentary Geology 95, 147–160. DOI:10.1016/0037-0738(94)00122-B

Japsen, P., Green, P.F., Bonow, J.M., Hinchey, A.M., Wilton, D.H.C., 2016. Burial and exhumation history of the Labrador- Newfoundland margin: first observations. Geological Survey of Denmark and Greenland Bulletin 35, 91-94. DOI:10.4043/27379-MS

Joussiaume, R., 2016. Les relations entre diapirisme et sédimentation: Exemple du Jurassique moyen de la région d'Imilchil, Haut-Atlas central, Maroc. Thèse de doctorat de l'université Bordeaux Montaigne. 308 pp.

Kerr, D.R., 1984. Early neogene continental sedimentation in the vallecito and fish creek mountains, Western Salton Trough, California. Sedimentary geology, *38*(1-4), pp.217-246. DOI: 10.1016/0037-0738(84)90080-0

Kluge C., 2016. A Structural Modeling Approach on Timing & Evolution of Mesozoic Anticlines in the Western High Atlas, Morocco. Master thesis, Delft University.

Knaust, D., 2013. The ichnogenus Rhizocorallium: Classification, trace makers, palaeoenvironments and evolution. Earth-Science Reviews, 126, 1–47. DOI:10.1016/j.earscirev.2013.04.007

Knight, K. B., Nomade, S., Renne, P. R., Marzoli, A., Bertrand, H., Youbi, N., 2004. The Central Atlantic magmatic province at the Triassic–Jurassic boundary: paleomagnetic and 40Ar/39Ar evidence from Morocco for brief, episodic volcanism. Earth and Planetary Science Letters 228, 143-160. DOI:10.1016/j.epsl.2004.09.022

Lachkar, N., 2000. Dynamique sédimentaire d'un bassin extensif sur la marge Sud téthysienne: le Lias du Haut-Atlas de Rich (Maroc). These de Doctorat, Université de Bourgogne, Dijon, 275 pp.

Lanari, R., Faccenna, C., Fellin, M.G., Essaifi, A., Nahid, A., Medina, F. and Youbi, N., 2020. Tectonic Evolution of the Western High Atlas of Morocco: Oblique Convergence, Reactivation, and Transpression. Tectonics, 39. DOI: 10.1029/2019TC005563

Laville, E., and Petit, J., 1984. Role of synsedimentary strike-slip faults in the formation of Moroccan Triassic basins. *Geology* *12*(7). DOI:10.1130/0091-7613(1984)12<424:ROSSFI>2.0.CO;2

Laville, E., Pique, A., 1992. Jurassic Penetrative Deformation and Cenozoic Uplift in the Central High Atlas (Morocco): A Tectonic Model. Structural and Orogenic Inversions: Geologische Rundschau 81, 157–170. DOI:10.1007/BF01764546

Laville, E., Pique, A., Amrhar, M., Charroud, M., 2004. A restatement of the Mesozoic Atlasic Rifting (Morocco). Journal of African Earth Sciences 38(2), 145–153. DOI:10.1016/j.jafrearsci.2003.12.003

Lehner P., De Ruiter P.A.C., 1977. Structural history of Atlantic Margin of Africa. American Association of Petroleum Geology, Bulletin 61, 961-981. DOI:10.1306/C1EA43B0-16C9-11D7-8645000102C1865D

Le Roy P., 1997. Les bassins ouest-marocains; leur formation et leur évolution dans le cadre de l'ouverture et du développement de l'Atlantique central (marge africaine), Thèse de l'Université de Bretagne occidentale, Brest, 326pp.

Le Roy P., Piqué A., 2001. Triassic-Liassic Western Morocco synrift basins in relation to the Central Atlantic opening. Marine Geology 172, 359–381. DOI:10.1016/S0025-3227(00)00130-4

Lowe, D.R., 1988. Suspended-load fallout rate as an independent variable in the analysis of current structures. Sedimentology, 35(5), 765-776. DOI: 10.1111/j.1365-3091.1988.tb01250.x

Lu, F., Meyers, W., 1998. Massive dolomitization of a late Miocene carbonate platform: a case of mixed evaporative brines with meteoric water, Nijar, Spain. Sedimentology 45(2), 263–277. Doi: 10.1046/j.1365-3091.1998.0142e.x

Lunt, I., and Bridge, J., 2004. Evolution and deposits of a gravelly braid bar, Sagavanirktok River, Alaska. Sedimentology, 51(3), 415–432. DOI:10.1111/j.1365-3091.2004.00628.x

Mader, N., Redfern, J., 2011. A sedimentological model for the continental Upper Triassic Tadrart Ouadou Sandstone Member: recording an interplay of climate and tectonics (Argana Valley; South-west Morocco). Sedimentology 58(5), 1247–1282. DOI:10.1111/j.1365-3091.2010.01204.x

Malaval, M., 2016. Enregistrement sédimentaire de l'activité diapirique associée à la ride du Jbel Azourki Haut-Atlas Central, Maroc. Thèse de doctorat de l'université Bordeaux Montaigne, 383 pp.

Martin, A.J., 2000. Flaser and wavy bedding in ephemeral streams: a modern and an ancient example. Sedimentary Geology, 136(1-2), 1-5. DOI: 10.1016/S0037-0738(00)00085-3

Martín-Martín, J., Vergés, J., Saura, E., Moragas, M., Messager, G., Baqués, V., Razin, P., Grélaud, C., Malaval, M., Joussiaume, R., Casciello, E., Cruz-Orosa, I., Hunt, D., 2017. Diapiric growth within an Early Jurassic rift basin: The Tazoult salt wall (central High Atlas, Morocco). Tectonics 36(1), 2–32. DOI:10.1002/2016TC004300

Marzoli, A., Bertrand, H., Knight, K.B., Cirili, S., Buratti, N., Verati, C., Nomade, S., Renne, P.R., Youbi, N., Martini, R., Allenbach, K., Neuwerth, R., Rapaille, C., Zaninetti, L., Bellieni, G., 2004. Synchrony of the Central Atlantic magmatic province and the Triassic-Jurassic boundary climatic and biotic crisis: Geology 32(11), 973–976. DOI:10.1130/G20652.1

Marzoli, A., Renne, P. R., Piccirillo, E. M., Ernesto, M., Bellieni, G., De Min, A., 1999. Extensive 200 million-year-old continental flood basalts of the Central Atlantic Magmatic Province. Science 284, 616–618. DOI:10.1126/science.284.5414.616

McCarthy, P.J., Martini, I.P. and Leckie, D.A., 1997. Anatomy and evolution of a Lower Cretaceous alluvial plain: sedimentology and palaeosols in the upper Blairmore Group, south-western Alberta, Canada. Sedimentology, 44(2), 197-220. DOI: 10.1111/j.1365-3091.1997.tb01521.x

Medina, F., 1988. Tilted-blocks pattern, paleostress orientation and amount of extension, related to Triassic early rifting of the Central Atlantic in the Arnzri area (Argana basin, Morocco). Tectonophysics 148, 229-233. DOI:10.1016/0040-1951(88)90131-X

Miall, A. D., 1977. A review of the braided river depositional environment. Earth Science Reviews 13, 1-62. DOI:10.1016/0012-8252(77)90055-1

Miall, A. D., 1996. The Geology of Fluvial Deposits. Springer-Verlag, Berlin, 582 pp. DOI:10.1007/978-3-662-03237-4

Miall, A. D., 2006. The Geology of Fluvial Deposits: Sedimentary Facies, Basin Analysis, and Petroleum Geology. Springer-Verlag, Berlin, 582 pp. DOI:10.1007/978-3-662-03237-4

Moragas, M., Vergés, J., Saura, E., Martín-Martín, J.-D., Messager, G., Merino-Tomé, Ó., Suárez-Ruiz, I. , Razin, P., Grélaud, C., Malaval, M., Joussiaume, R., Hunt, D.W., 2016. Jurassic rifting to post-rift subsidence analysis in the Central High Atlas and its relation to salt diapirism. Basin Res. (2016), pp. 1-27. DOI:10.1111/bre.12223

Moragas, M., Vergés, J., Nalpas, T., Saura, E., Martín-Martín, J., Messager, G., & Hunt, D., 2017. The impact of syn- and post-extension prograding sedimentation on the development of salt-related rift basins and their inversion: Clues from analogue modelling. Marine and Petroleum Geology, 88, 985–1003. DOI:10.1016/j.marpetgeo.2017.10.001

Moragas, M., Vergés, J., Saura, E., Martín-Martín, J., Messager, G., Merino-Tomé, Ó., Suárez-Ruiz, I., Razin, P., Grélaud, C., Malaval, M., Joussiaume, R., Hunt, D., 2018. Jurassic rifting to post-rift subsidence analysis in the Central High Atlas and its relation to salt diapirism. Basin Research., 30, 336–362. DOI:10.1111/bre.12223

Muñoz, A., Ramos, A., Sánchez-Moya, Y., Sopeña, A., 1992. Evolving fluvial architecture during a marine transgression: Upper Buntsandstein, Triassic, central Spain. Sedimentary Geology 75(3-4), 257–281. DOI:10.1016/0037-0738(92)90096-A

Murray, R.C., 1964. Origin and diagenesis of gypsum and anhydrite. Journal of Sedimentary Research, 34(3), 512-523. DOI: 10.1306/74D710D2-2B21-11D7-8648000102C1865D

Nanson, G., 1980. Point bar and floodplain formation of the meandering Beatton River, northeastern British Columbia, Canada. Sedimentology 27(1), 3–29. DOI:10.1111/j.1365-3091.1980.tb01155.x

Nemec, W., Postma, G., 1993. Quaternary alluvial fans in southwestern Crete: sedimentation processes and geomorphic evolution, in Marzo, M., and Puigdefábregas, C., (Editors), Alluvial Sedimentation: International Association of Sedimeotologists Special Publication 17, 235- 276. DOI:10.1002/9781444303995.ch18

Nilsen, T. H., 1982. Alluvial fan deposits, in Sandstone depositional environments: Tulsa, Oklahoma, American Association of Petroleum Geologists. 49–86.

Nomade, S., Knight, K.B., Beutel, E., Renne, P.R., Verati, C., Féraud, G., Marzoli, a., Youbi, N., Bertrand, H., 2007. Chronology of the Central Atlantic Magmatic Province: Implications for the Central Atlantic rifting processes and the Triassic-Jurassic biotic crisis: Palaeogeography, Palaeoclimatology, Palaeoecology 244(1–4), 326–344. DOI:10.1016/j.palaeo.2006.06.034

Olsen, P.E., Kent, D. V., Et-Touhami, M., Puffer, J., 2003. Cyclo-, magneto-, and bio-stratigraphic constraints on the duration of the CAMP event and its relationship to the triassic-jurassic boundary: Geophysical Monograph Series, American Geophysical Union, Washington, DC, 136, 7–32. DOI:10.1029/136GM02

Palfy, J., Smith, P.L., Mortensen, J.K., 2000. A U-Pb and Ar-40/Ar-39 time scale for the Jurassic: Canadian Journal of Earth Sciences 37(6), 923–944. DOI:10.1139/e00-002

Peybernès, B., Bouaouda, M.S., Alméras, Y., Ruget, C., Cugny, P., 1987. Stratigraphie du Lias et du Dogger du bassin côtier d'Essaouira (Maroc) avant et pendant le début de l'expansion océanique dans l'Atlantique central. Comparaison avec le bassin d'Agadir. Comptes-Rendus de l'Académie des Sciences, Paris, 305, 1449-1455.

Piqué, A., Le Roy, P., Amrhar, M., 1998. Transtensive synsedimentary tectonics associated with ocean opening: the Essaouira–Agadir segment of the Moroccan Atlantic margin. Journal of the Geological Society 155(6), 913–928. DOI:10.1144/gsjgs.155.6.0913

Plint, A., Nummedal, D., 2000. The falling stage systems tract: recognition and importance in sequence stratigraphic analysis. Geological Society Special Publication 172(1), 1–17. DOI:10.1144/GSL.SP.2000.172.01.01

Posamentier, H.W., Vail, P. R., 1988. Eustatic controls on clastic deposition. II. Sequence and systems tract models. In: Wilgus, C. K., Hastings, B. S., Kendall, C. G. St. C., Posamentier, H.W., Ross, C. A., Van Wagoner, J. C. (Editors.), Sea Level Changes - An Integrated Approach. SEPM Special Publication 42, 125–154. DOI:10.2110/pec.88.01.0125

Riegraf, W., Luterbacher, H., and Leckie, R.M., 1984. Jurassic Foraminifers from the Mazagan Plateau, Deep Sea Drilling Project Site 547, Leg 79, off Morocco. Initial Report Deep Sea Drilling Project, Washington, 79 (13), 671-702. DOI:10.2973/dsdp.proc.79.1984

Roch, E., 1930. Étude géologique dans la région méridionale du Maroc occidental. Notes et Mémoires du Service géologique du Maroc, Rabat, 9, 1–542.

Rouchy, J., Caruso, A., 2006. The Messinian salinity crisis in the Mediterranean basin: A reassessment of the data and an integrated scenario. Sedimentary Geology, 188, 35–67. DOI:10.1016/j.sedgeo.2006.02.005

Rust, B. R., 1972. Structure and process in a braided river. Sedimentology, 18(3-4), 221–245. DOI:10.1111/j.1365-3091.1972.tb00013.x

Rust, B. R., 1977, A classification of alluvial channel systems, In Miall (Editor), Fluvial Sedimentology. Canadian Society of Petroleum Geology, Calgary, Alberta, 669-702. DOI:10.1002/esp.3760050213

Saddiqi, O., Haimer, El, F.Z., Michard, A., Barbarand, J., Ruiz, G.M.H., Mansour, E.M., Leturmy, P. Frizon de Lamotte, D., 2009. Apatite fission-track analyses on basement granites from south-western Meseta, Morocco: Paleogeographic implications and interpretation of AFT age discrepancies. Tectonophysics 475, 29–37. DOI:10.1016/j.tecto.2009.01.007

Saura, E., Verges, J., Martin-Martin, J.D., Messager, G., Moragas, M., Razin, P., Grelaud, C., Joussiaume, R., Malaval, M., Homke, S., Hunt, D.W., 2014. Syn- to post-rift diapirism and minibasins of the Central High Atlas (Morocco): The changing face of a mountain belt: Journal of the Geological Society 171, p. 97–105. DOI:10.1144/jgs2013-079

Schettino, A., Turco, E., 2009. Breakup of Pangaea and plate kinematics of the central Atlantic and Atlas regions. Geophysical Journal International 178(2), 1078–1097. DOI:10.1111/j.1365-246X.2009.04186.x

Schettino, A., Turco, E., 2011. Tectonic history of the western Tethys since the Late Triassic. Geological Society of America Bulletin 123(1-2), 89–105. DOI:10.1130/B30064.1

Sehrt, M., 2014. Variscan to Neogene long-term landscape evolution at the Moroccan passive continental margin (Tarfaya Basin and western Anti-Atlas): University of Heidelberg, Ph.D. Thesis, 174pp. DOI:10.11588/heidok.00017463

Semeniuk, V., 1996. Coastal forms and Quaternary processes along the arid Pilbara coast of northwestern Australia. Palaeogeogr. Palaeoclimatol. Palaeoecol. 123 (1–4), 49–84. https://doi.org/10.1016/0031-0182(96)00103-4.

Silva, P.F., Marques, F.O., Henry, B., Madureira, P., Hirt, A.M., Font, E., Lourenço, N., 2010. Thick dyke emplacement and internal flow: A structural and magnetic fabric study of the deep-seated dolerite dyke of Foum Zguid (southern Morocco). J. Geophys. Res. Solid Earth 115 (B12). https://doi.org/10.1029/2010jb007638.

Smith, R. M. H., 1980. The lithology, sedimentology and taphonomy of flood-plain deposits of the Lower Beaufort (Adelaide Subgroup) strata near Beaufort West. South African Journal of Geology 83(3), 399 pp.

Snedden, J.W., Liu, C. 2011. Recommendations for uniform chronostratigraphic designation system for Phanerozoic depositional sequences. AAPG bulletin 95, 1095-1122. DOI:10.1306/01031110138

Steiger, T., and Jansa, L. F., Jurassic Limestones of the Seaward Edge of the Mazagan Carbonate Platform, Northwest African Continental Margin, Morocco. Initial Report Deep Sea Drilling Project, Washington, 79 (13), 449-491. DOI:10.2973/dsdp.proc.79.1984

Stets, J., 1992. Mid-Jurassic events in the Western High Atlas (Morocco). International Journal of Earth Sciences 81(1), 69–84. DOI:10.1007/BF01764540

Strasser, A., 1988. Shallowing-upward sequences in Purbeckian peritidal carbonates (lowermost Cretaceous, Swiss and French Jura Mountains). Sedimentology, 35(3), pp.369-383. DOI:10.1111/j.1365-3091.1988.tb00992.x

Teixell, A., Barnolas, A., Rosales, I., and Arboleya, M., 2017. Structural and facies architecture of a diapir-related carbonate minibasin (lower and middle Jurassic, High Atlas, Morocco). Marine and Petroleum Geology 81, 334–360. DOI:10.1016/j.marpetgeo.2017.01.003

Terwindt, J. H. J., 1988. Palaeo-tidal reconstructions of inshore tidal depositional environments. In P. L. de Boer et al (Editors), Tide-influenced sedimentary environments and facies. Reidel Dordrecht, 233-263.

Tixeron, M., 1974. Carte géologique et minéralisations de couloir d'Argana. Notes et Memoires du Service Géologique du Maroc, 205.

Touil, A., Vegas, R., Hafid, A., Palomino, R., Rizki, A., Palencia-Ortas, A., Ruiz-Martınez, V.C., 2008. Petrography, mineralogy and geochemistry of the Ighrem diabase dyke (Anti-Atlas, Southern Morocco). Revista de la Sociedad Geológica de España 21(1-2), 25-33.

Tucker, M., 2001. Sedimentary Petrology–An Introduction to the Origin of Sedimentary Rocks .− Blackwell. Scientific publication, London. Tucker, M., 2009. Carbonate sedimentology. Oxford; Blackwell Scientific Publications, 482 pp. DOI:10.1002/9781444314175

Tucker, M., 2009. Carbonate Sedimentology. Oxford; Blackwell Scientific Publications, p. 482. https://doi.org/10.1002/9781444314175.

Tucker, M., 2011. Sedimentary Rocks in the Field : a Practical Guide. John Wiley & Sons, Ltd.

Tunbridge, I., 1984. Facies model for a sandy ephemeral stream and clay playa complex; the Middle Devonian Trentishoe Formation of North Devon, U.K. Sedimentology 31(5), 697–715. DOI:10.1111/j.1365-3091.1984.tb01231.x

Van Wagoner, J. C., Posamentier, H.W., Mitchum, R. M., Vail, P. R., Sarg, J. F., Loutit, T. S., Hardenbol, J., 1988. An overview of the fundamentals of sequence stratigraphy and key definitions. In: Wilgus, C. K., Hastings, B. S., Kendall, C. G. St. C., Posamentier, H.W., Ross, C. A., Van Wagoner, J. C. (Editors), Sea Level Changes – An Integrated Approach SEPM Special Publication 42, 39–45. DOI:10.2110/pec.88.01.0039

Verati, C., Rapaille, C., Féraud, G., Marzoli, A., Bertrand, H., Youbi, N., 2007. Ar / 39 Ar ages and duration of the Central Atlantic Magmatic Province volcanism in Morocco and Portugal and its relation to the Triassic-Jurassic boundary. Palaeogeography, Palaeoclimatology, Palaeoecology 244, 308–325. DOI:10.1016/j.palaeo.2006.06.033

Vergés, J., Moragas, M., Martín-Martín, J., Saura, E., Casciello, E., Razin, P., Grelaud, C., Malaval, M., Joussiame, R., Messager, G., Sharp, I., Hunt, D. 2017. Salt Tectonics in the Atlas Mountains of Morocco. In Permo-triassic salt provinces of Europe, North Africa and the Atlantic margins : tectonics and hydrocarbon potential. 563–579. DOI:10.1016/B978-0-12-809417-4.00027-6

Warren, J. K., 1991. Sulfate Dominated Sea-Marginal and Platform Evaporative Settings: Evaporites, petroleum and mineral resources. Developments in Sedimentology 50, 69–187). DOI:10.1016/S0070-4571(08)70260-7

Warren, J. K., 2016. Evaporites: A geological compendium. Springer, 1813 pp. DOI:10.1007/978-3-319-13512-0

Wentworth, C.K., 1922. A scale of grade and class terms for clastic sediments. The journal of geology, 30(5), 377-392.

West, I.M., Ali, Y.A. and Hilmy, M.E., 1979. Primary gypsum nodules in a modern sabkha on the Mediterranean coast of Egypt. Geology, 7(7), 354-358. DOI: 10.1130/0091-7613(1979)7<354:PGNIAM>2.0.CO;2

Whiteside, J.H., Olsen, P.E., Kent, D. V, Fowell, S.J., and Et-touhami, M., 2007. Synchrony between the Central Atlantic magmatic province and the Triassic-Jurassic mass-extinction event? Palaeogeography, Palaeoclimatology, Palaeoecology 244, 345–367. DOI:10.1016/j.palaeo.2006.06.035.

Wildman, M., Brown, R., Watkins, R., Carter, A., Gleadow, A., Summerfield, M., 2015. Post break-up tectonic inversion across the southwestern cape of South Africa: New insights from apatite and zircon fission track thermochronometry. Tectonophysics 654, 30-55. DOI:10.1016/j.tecto.2015.04.012

Williams, P. F. and Rust, B., 1969. The Sedimentology of a Braided River. Journal of Sedimentary Research., Vol. 39. DOI:10.1306/74D71CF3-2B21-11D7-8648000102C1865D

Wilmsen, M. Et Neuweiler, F., 2008. Biosedimentology of the Early Jurassic post-extinction carbonate depositional system, central High Atlas rift basin, Morocco. Sedimentology 55(4), 773-807. DOI:10.1111/j.1365-3091.2007.00921.x

Wilson, A., Flint, S., Payenberg, T., Tohver, E. and Lanci, L., 2014. Architectural styles and sedimentology of the fluvial lower Beaufort Group, Karoo Basin, South Africa. Journal of Sedimentary Research, 84(4), 326-348. DOI: http://dx.doi.org/10.2110/jsr.2014.28

Zonneveld, J.P., Gingras, M.K., Pemberton, S.G., 2001. Trace fossil assemblages in a Middle Triassic mixed siliciclastic-carbonate marginal marine depositional system, British Columbia. Palaeogeogr. Palaeoclimatol. Palaeoecol. 166 (3–4), 249–276. https://doi.org/10.1016/S0031-0182(00)00212-1